



The AquaVIT-4 intercomparison of atmospheric hygrometers

Simone Brunamonti¹, Harald Saathoff², Albert Hertzog³, Glenn Diskin⁴, Masatomo Fujiwara⁵, Karen Rosenlof⁶, Ottmar Möhler², Béla Tuzson¹, Lukas Emmenegger¹, Nadir Amarouche⁷, Georges Durry³, Fabien Frérot⁷, Jean-Christophe Samake⁷, Claire Cenac³, Julio Lopez³, Paul Monnier³, and Mélanie Ghysels⁸

¹Laboratory for Air Pollution/Environmental Technology, Empa, 8600 Dübendorf, Switzerland

²Institute of Meteorology and Climate Research – Atmospheric Aerosol Research, Karlsruhe Institute of Technology, 76344 Eggenstein-Leopoldshafen, Germany

³Laboratoire de Météorologie Dynamique, IPSL, Sorbonne Université, Ecole Polytechnique, 91 128 Palaiseau, France

⁴NASA Langley Research Center, Hampton, VA 23681, USA

⁵Faculty of Environmental Earth Science, Hokkaido University, Sapporo, 060-0810, Japan

⁶NOAA Chemical Sciences Laboratory, CSL-8, Boulder, CO 80305, USA

⁷INSU Division Technique, 1 avenue de la terrasse, 91190 Gif-sur-Yvette, France

⁸Groupe de Spectrométrie Moléculaire et Atmosphérique, Université de Reims, CNRS, UFR Sciences Exactes et Naturelles, Moulin de la Housse B.P. 1039, 51687 Reims Cedex 2, France

Correspondence: Mélanie Ghysels (melanie.ghysels-dubois@cnrs.fr)

Received: 4 March 2025 – Discussion started: 28 April 2025

Revised: 16 July 2025 – Accepted: 30 July 2025 – Published: 15 October 2025

Abstract. The AquaVIT-4 intercomparison of atmospheric hygrometers was conducted at the AIDA (Aerosol Interaction and Dynamics in the Atmosphere) climate simulation chamber of the Karlsruhe Institute of Technology (KIT), Germany, in March–April 2022, within the framework of the HEMERA H2020 EU project. The objectives were to document the performance of existing hygrometers and to support the development of novel methods for water vapor (H₂O) measurements in the upper atmosphere. The AquaVIT-4 intercomparison involved seven hygrometers based on either infrared laser absorption spectroscopy or frost-point hygrometry techniques: four deployed on aircraft or stratospheric balloon platforms and three reference instruments. The simulated conditions in the AIDA chamber reproduced the characteristic atmospheric conditions of the upper troposphere–lower stratosphere (UTLS, altitude range ~ 5 –28 km) in the tropics and midlatitudes, spanning 20–600 hPa pressure, 190–245 K temperature, and 0.5–530 ppm H₂O mixing ratio. The campaign was divided into two phases, each consisting of 4 measurement days: an “open intercomparison”, where the simulated conditions were known to the participants, and a “blind intercomparison”, where the conditions were coordinated by independent referees and unknown to the participating teams. Here we present a statistical analysis of the

entire dataset, which allows us to assess the accuracy and limitations of each instrument. For the accuracy evaluation, two sets of reference measurements were defined: one for in situ instruments, located inside the AIDA vessel, and one for extractive instruments, sampling the chamber gas through a heated inlet. This distinction accounts for H₂O desorption effects, which are most prominent at low pressures and low H₂O concentrations. All instruments showed good agreement with the reference values in the range of H₂O > 2 ppm, with mean deviations within $\pm 7\%$ for H₂O > 10 ppm and $\pm 8\%$ between 2–10 ppm H₂O. The largest differences were found for H₂O < 2 ppm, a rarely observed range in the atmosphere, though most of the instruments still achieved average deviations within $\pm 10\%$. Overall, the results of AquaVIT-4 demonstrate the high accuracy and reliability of the four involved sensors for upper-atmospheric monitoring and research applications.

1 Introduction

Water vapor (H_2O) is a strong greenhouse gas that substantially contributes to the Earth's radiative balance. Radiative–convective models and observations have shown that increasing greenhouse gases like CO_2 can lead to a moistening of the troposphere (Soden et al., 2005; Dessler et al., 2008, 2013), potentially doubling the warming effect of CO_2 (Banerjee et al., 2019; Dessler et al., 2013). Dessler et al. (2013) demonstrated a link between interannual variations in tropospheric temperature and the amount of H_2O entering the stratosphere, suggesting a stratospheric water vapor climate feedback of about $+0.3 \text{ W m}^{-2} \text{ K}^{-1}$ (see also Forster et al., 2021, for an overview of the topic). Observational studies showed that stratospheric moistening can lead to an increase in the mean surface temperature (Forster and Shine, 1999; Riese et al., 2012; Solomon et al., 2010), with disparities across different latitudes. Additionally, stratospheric H_2O affects the atmospheric circulation (Maycock et al., 2014) and stratospheric ozone chemistry (Stenke and Grewe, 2005).

In situ measurements by the NOAA frost-point hygrometer (FPH) reported a 1 %–1.5 % annual increase in stratospheric H_2O (16–28 km altitude) between 1980 and 2000 (Oltmans et al., 2000). Using multiple datasets, Rosenlof et al. (2001) found a persistent trend of 1 % annual increase in stratospheric H_2O from 1954 to 2000, later revised to 0.6 \% yr^{-1} (Scherer et al., 2008). Statistically significant positive trends of stratospheric H_2O were also found by Hurst et al. (2011, 2022), along with short-term variability driven by cold-point tropopause (CPT) temperature variations (e.g., Randel and Park, 2019) and large-scale stratospheric dynamics, such as the Brewer–Dobson circulation (Tao et al., 2023) and the quasi-biennial oscillation (Tian et al., 2019). The analysis of a composite of satellite observations showed negative trends in H_2O in the lower and mid-stratosphere and positive trends in the upper stratosphere due to methane oxidation (Hegglin et al., 2013; Tao et al., 2023).

In the upper troposphere and lower stratosphere (UTLS, altitude range ~ 5 –28 km), and in particular above the tropopause, typical mixing ratios of H_2O are $< 10 \text{ ppm}$ (parts per million, i.e., $\mu\text{mol mol}^{-1}$). High-resolution measurements above 15 km are primarily obtained from instruments carried on stratospheric balloons or aboard high-altitude aircraft, while satellite observations provide vertical profiling with 1.5–3 km resolution and extensive spatial and temporal coverage (e.g., Hegglin et al., 2013; Hurst et al., 2014, 2016). Although this allows us to address large-scale processes, the use of in situ instruments aboard balloons or aircraft remains essential for resolving microphysical processes and validating satellite observations. In particular, high-resolution observations are crucial for studying H_2O transport and dehydration processes in the UTLS, such as fine cirrus layer formation near the tropopause (e.g., Luo et al., 2003; Peter et al., 2006). Numerical weather prediction (NWP) models largely benefit from water vapor observations in the UTLS

in validating their models as stratospheric H_2O is not assimilated. Discrepancies up to $\pm 17 \text{ \%}$ have been found between operational and re-analysis (ERA5) data from the European Centre for Medium-Range Weather Forecasts (ECMWF) and balloon-borne measurements (Brunamonti et al., 2019).

Upper-air H_2O is classified as an essential climate variable (ECV) by the Global Climate Observing System (GCOS), with revised measurement requirements (GCOS, 2022). Particularly, the minimum threshold for useful measurements in terms of climate monitoring studies is set to 0.5 ppm ($\sim 10 \text{ \%}$) at 250 m vertical resolution, whereas the “goal” level, for which no further improvement is necessary, is set to 0.1 ppm ($\sim 2 \text{ \%}$) at 10 m resolution. Currently, routine measurements of UTLS H_2O in the GCOS Reference Upper Air Network (GRUAN) are performed by balloon-borne cryogenic frost-point hygrometry (CFH/FPH). These instruments are based on the chilled-mirror principle and have an estimated uncertainty of 4 %–6 % in the UTLS (Hall et al., 2016; Vömel et al., 2016). However, these devices are being re-designed due to the phase-out of the cooling agent fluoroform (HFC-23) used for their operation because of its high global warming potential (UNEP, 2016). Alternative cooling solutions, such as the use of liquid nitrogen or a mix of dry ice and alcohol, are currently being implemented and validated (e.g., Rolf et al., 2020; Dirksen, 2024; Poltera et al., 2025).

Despite their importance, accurate in situ measurements of UTLS H_2O remain highly challenging, with substantial discrepancies between different techniques. Comparison between Lyman- α fluorescence (e.g., Zöger et al., 1999; Sitenikov et al., 2007) and CFH measurements showed differences within $\pm 10 \text{ \%}$ between 11–20 km altitude and up to 30 % outside this range (Vömel et al., 2007). Rollins et al. (2014) found differences as large as 20 % between airborne Lyman- α , laser spectroscopy and mass spectrometry instruments, and balloon-based CFH measurements during the MACPEX campaign. Kaufmann et al. (2018) reported deviations as large as 20 % for $\text{H}_2\text{O} < 10 \text{ ppm}$ between Lyman- α and mass spectrometry instruments on board the HALO aircraft. Ghysels et al. (2016) compared the Pico-SDLA H_2O spectrometer with Lyman- α in the tropical UTLS (15–23 km altitude), finding differences up to $1.9 \pm 9.0 \text{ \%}$ above the CPT. Singer et al. (2022) reported good agreement between off-axis integrated cavity output spectrometry and Lyman- α instruments on board the Geophysica M-55 aircraft and balloon-borne CFH measurements during the StratoClim airborne campaign in the Asian UTLS. A recent study by Ghysels et al. (2024) compared the Pico-Light H_2O hygrometer with the NOAA FPH in the midlatitudes and found agreement of $4.2 \pm 2.7 \text{ \%}$ in the UTLS.

Considering the above findings, rigorous intercomparisons are of critical importance to allow a valuable scientific interpretation and quality assessment of the measured data (e.g., Krämer et al., 2009). Over the past two decades, this led to the organization of a series of international hygrometer intercomparisons, known as the AquaVIT, held at the AIDA

(Aerosol Interaction and Dynamics in the Atmosphere) climate simulation chamber of the Karlsruhe Institute of Technology (KIT), Germany, and aimed to clarify the uncertainties in UTLS H₂O measurements and to identify the causes of the observed discrepancies. The first AquaVIT-1 intercomparison (Fahey et al., 2014) was conducted in October 2007 at the AIDA chamber, testing more than 20 different water vapor sensors subject to a wide range of environmental conditions (pressure 50–500 hPa, temperature 185–243 K, H₂O mixing ratio 0.3–152 ppm). Given the absence of an accepted reference measurement, the accuracy of the instruments was established with respect to the ensemble mean of a “core” subset of instruments. While many instruments were found to differ from such a reference by $\pm 100\%$ or more, the “core” instruments showed variations smaller than $\pm 10\%$ relative to the reference value under all conditions (Fahey et al., 2014). The AquaVIT-2 intercomparison was conducted in April 2013 and the results have been reported individually for some of the participating instruments (Meyer et al., 2015; Hall et al., 2016). AquaVIT-3 was conducted in July 2015 with aircraft instruments and new onboard calibration units. The AquaVIT series assessed the quality of major atmospheric hygrometers and documented their improvements over time, facilitated by information exchange during the intercomparison campaigns.

As a continuation of these efforts, the AquaVIT-4 campaign was conceived and conducted in March–April 2022 at the AIDA chamber, within the HEMERA H2020 EU project. The intercomparison featured in total seven hygrometers based on either direct infrared laser absorption spectroscopy or frost-point hygrometry techniques: four designed to be deployed on aircraft or stratospheric balloon platforms and three reference instruments. The simulated conditions in the AIDA chamber were focused on reproducing the characteristic atmospheric conditions of the tropical and midlatitude UTLS (pressure 20–600 hPa, temperature 190–245 K, H₂O mixing ratio 0.5–530 ppm).

Here we present the results of the AquaVIT-4 measurement campaign and assess the accuracy and limitations of the participating instruments. The AIDA chamber facility and the individual instruments are described in Sects. 2–3. The strategy of the intercomparison and the simulated conditions are presented in Sect. 4. The statistical analysis of the results is discussed in Sects. 5–6. Detailed descriptions of the data processing algorithms and instrument-specific issues are provided in the Appendix.

2 AIDA chamber

The Aerosol Interaction and Dynamics in the Atmosphere (AIDA) chamber, located at the Karlsruhe Institute of Technology (KIT, Germany), is an aluminum vessel of 84 m³ volume, with the possibility to control pressure from 1100 to 0.01 hPa and temperature from 313 to 183 K (Möhler et

al., 2003; Wagner et al., 2009; Skrotzki et al., 2013). A mixing fan inside the AIDA chamber provides homogeneity throughout the chamber volume within 90 s. This allows simulating atmospheric conditions relevant for aerosol and cloud formation processes under tropospheric and lower-stratospheric conditions on timescales of minutes to hours. Over the past two decades, the AIDA chamber was used in a large number of studies investigating atmospheric aerosols and clouds (Wagner et al., 2006, Möhler et al., 2008, Donahue et al., 2012, Skrotzki et al., 2013, Lamb et al., 2017, Gao et al., 2022), as well as to test and compare the performance of research instruments to be deployed in field campaigns (Laborde et al., 2012, Shen et al., 2024), including atmospheric hygrometers. Most notably, the AIDA chamber hosted the previous three intercomparison campaigns of the AquaVIT series, including AquaVIT-1 (Fahey et al., 2014), involving more than 20 different atmospheric hygrometers, and AquaVIT-2 with a focus on traceability to national standards (Buchholz et al., 2014, Hall et al., 2016) as well as AquaVIT-3 testing aircraft instruments and onboard calibration units. The work presented here heavily relies on the AquaVIT-1 experience for the experimental design and integration of the different sensors into the AIDA chamber facility.

The key features of the AIDA chamber for the AquaVIT intercomparisons include (i) operation at near-constant pressure (± 1 hPa) and temperature (± 0.3 K) conditions, (ii) the possibility to vary the H₂O mixing ratio, concentration, and relative humidity by addition of H₂O or dry air and/or the partial removal of chamber air by pumping, and (iii) large chamber volume with small surface-wall-to-volume ratio, allowing multiple instruments to be located inside the chamber or to sample air from outside the chamber without significantly disturbing internal conditions (Fahey et al., 2014). Conditions (i–ii) allow the H₂O mixing ratio in the chamber to be constant or slowly changing for long periods of time (up to ~ 1 h), thereby allowing adequate time for all instruments to sample chamber air and make multiple determinations of water vapor content. Condition (iii) facilitates the use of customized, extractive sampling probes to deliver chamber air to instruments located outside the chamber. As in AquaVIT-1 (Fahey et al., 2014), the probes used here consisted of electropolished stainless-steel tubing and were heated to reduce water adsorption and to evaporate droplets.

3 Instruments and configuration

The AquaVIT-4 intercomparison featured in total seven atmospheric hygrometers (four participants and three reference instruments) based on either direct infrared laser absorption spectroscopy or frost-point hygrometry, which were tested in the AIDA chamber under a wide range of pressures, temperatures, and humidities, simulating the characteristic atmo-

spheric conditions for an altitude range of approximately 5–28 km, from the midlatitudes to tropical latitudes.

The participating instruments included (in alphabetical order) a balloon-borne laser absorption spectrometer for UTLS water research (“ALBATROSS”) by Empa, Switzerland (Graf et al., 2021; Brunamonti et al., 2023); the Diode Laser Hygrometer (DLH) by NASA, USA (Diskin et al., 2002); the Pico-Light H₂O (Ghysels et al., 2024) by CNRS, France, successor of the former Pico-SDLA instrument (Durry et al., 2008); and the Surface Acoustic Wave frost-Point Hygrometer (SAWfPHY) by LMD, France. Reference instruments, all operated by KIT (Germany), included the AIDA-PCI-in-cloud-TDL (APicT) (Ebert et al., 2005), the single-path AIDA-PCI-in-cloud-TDL (SP-APicT) (Skrotzki, 2012; Sarkozy et al., 2020; Lamb et al., 2023), and the commercial chilled-mirror hygrometer MBW373LX by MBW Calibration AG (Switzerland). The main features and reported uncertainties of all instruments are summarized in Table 1.

Figure 1 illustrates the experimental setup and the installation location of the different instruments in the AIDA chamber. The instruments participating in AquaVIT-4 can be divided in two categories: internal (in situ) instruments, located either directly inside the AIDA vessel or within its thermostated enclosure, and external (extractive) instruments, probing the chamber air through a heated sampling line. Specifically, five instruments participating in AquaVIT-4 are classified as internal (Pico-Light H₂O, SAWfPHY, DLH, APicT, SP-APicT) and two as external (ALBATROSS, MBW373LX). The Pico-Light H₂O and SAWfPHY hygrometers were installed inside the main vessel of AIDA, separated by about 1 m of distance. The main optical components of APicT, SP-APicT, and DLH were located within the thermostated enclosure (outside the main vessel), while their optical beams were folded between the inner chamber walls, providing a measurement of the H₂O mixing ratio averaged over the full diameter of the chamber. Conversely, ALBATROSS and MBW373LX were located outside of the thermostated enclosure, sharing the same heated sampling line. The flow rate drawn by the two instruments varied between 0.3–1 standard liter per minute (SLM) for MBW373LX and 0.02–0.5 SLM for ALBATROSS, depending on AIDA pressure (see Appendix A3). This corresponds to a total removal of up to 0.002 % of the chamber volume per minute (~ 100 times smaller than in AquaVIT-1, Fahey et al., 2014).

3.1 ALBATROSS laser spectrometer

The balloon-borne laser absorption spectrometer for UTLS water research (“ALBATROSS”) is a compact (< 3.5 kg) mid-IR laser spectrometer developed by Graf et al. (2021). ALBATROSS incorporates a monolithic segmented circular multipass cell (Graf et al., 2018) that allows an optical path length of 6 m within a cell diameter of 10.8 cm. The multipass cell is highly resistant to thermally induced dis-

tortion and can be operated in both closed- and open-path configuration. A continuous-wave distributed-feedback mid-IR quantum-cascade laser (cw-DFB-QCL), tuned to a spectral window of ~ 1 cm⁻¹ centered around an isolated absorption line of H₂O at 1662.809 cm⁻¹ ($\lambda \approx 6.01 \mu\text{m}$), is used as a light source. ALBATROSS uses rapid spectral sweeping of the QCL by periodic modulation of the laser driving current. A highly energy-efficient strategy, referred to as “intermittent continuous-wave” (iCW) modulation (Fischer et al., 2014), is implemented, in which the driving current is applied in pulses, typically 200 μs long, followed by a short period of complete shutdown of the laser. The transmission data, consisting of 25×10^3 data points, are digitized by a 14-bit analog–digital converter (ADC) at 125 MSs⁻¹ and real-time-processed by an FPGA (STEMlab 125-14, Red Pitaya). The signal-to-noise ratio is further improved by averaging up to 3000 individual spectra in real time, leading to an effective measurement rate of 1 Hz. A full description of the laser driving and data acquisition systems can be found in Graf et al. (2021).

The accuracy and precision of ALBATROSS at UTLS-relevant conditions were validated using SI-traceable reference mixtures, generated by a dynamic–gravimetric permeation method established at the Swiss Metrological Institute, METAS (Brunamonti et al., 2023). It was demonstrated that ALBATROSS achieves an accuracy better than $\pm 1.5 \%$ at all investigated pressures (30–250 hPa) and H₂O mixing ratios (2.5–35 ppm) and a 1 s precision better than 30 ppb (i.e., 0.1 % at 35 ppm H₂O). The spectrometer also achieves a linear response within $\pm 1.5 \%$ up to 180 ppm H₂O (Brunamonti et al., 2023).

Recently, ALBATROSS was deployed in a series of atmospheric test flights conducted from the MeteoSwiss Payerne Observatory (Switzerland) in the framework of the Swiss H₂O-Hub project, in tandem with a CFH instrument as a reference. The results show good agreement within $\pm 10 \%$ between ALBATROSS and CFH up to about 30 hPa pressure (~ 24 km altitude).

For the AquaVIT-4 intercomparison, ALBATROSS was operated in a “closed-path” configuration, as described in Brunamonti et al. (2023), in which the sample gas is pumped from the AIDA chamber through a heated sampling line. A detailed description of the sampling system and the data processing algorithm is given in Appendix A3.

3.2 DLH (Diode Laser Hygrometer)

The NASA Langley Diode Laser Hygrometer (DLH) is an external, open-path, near-infrared tunable-diode laser absorption instrument which has flown on nine different aircraft since 1994 (Diskin, et al., 2002). There are several versions of DLH, as they are designed and constructed specifically for each aircraft; in general, each consists of a transmitter/receiver and a quasi-retroreflector, between which is the two-pass optical absorption path. Path lengths vary between

Table 1. Summary and main features of all instruments participating in the AquaVIT-4 intercomparison.

Instrument	Institute	Technique	Reported uncertainty	Sampling	Status
APicT	KIT, Germany	Tunable-diode laser absorption spectroscopy (TDLAS)	Accuracy < 5 %. 1 σ precision (2 s): ~ 25 ppb (from ~ 10 % at 0.25 ppm H ₂ O to 0.1 %–1 % at > 2 ppm H ₂ O), dynamic range 1–2000 ppm	In situ	Reference
SP-APicT	KIT, Germany	Tunable-diode laser absorption spectroscopy (TDLAS)	Accuracy < 5 % for > 100 ppm H ₂ O, dynamic range: 100–13000 ppm	In situ	Reference
MBW373LX	KIT, Germany	Dew-point mirror hygrometry	Accuracy \pm 0.1 K on frost-point temperature (T_{fp}) for range $T_{fp} > -95$ °C, corresponding to < 2 % in H ₂ O mixing ratio	Extractive	Reference
ALBATROSS	Empa, Switzerland	Quantum-cascade laser absorption spectroscopy (QCLAS)	Accuracy < 1.5 % for range 2.5–180 ppm H ₂ O, $p = 30$ –250 hPa*, 1 σ precision (1 s) ~ 30 ppb (~ 0.1 % at > 30 ppm H ₂ O)	Extractive	Participant
DLH	NASA, USA	Tunable-diode laser absorption spectroscopy (TDLAS)	Accuracy is the greater of 5 % or 0.5 ppm; precision (1 σ , 1 s) is greater of 0.1 % or 50 ppbv	In situ	Participant
Pico-Light H ₂ O	CNRS, France	Tunable-diode laser absorption spectroscopy (TDLAS)	Total uncertainty 12 % for $p < 45$ hPa, 7.5 % for $p = 45$ –70 hPa, 5.5 % for $p = 70$ –85 hPa, ~ 4 % for $p = 85$ –180 hPa, ~ 1.5 % for $p > 180$ hPa. Precision (1 s): 130 ppb.	In situ	Participant
SAWfPHY	LMD, France	Surface acoustic wave frost-point hygrometry	Accuracy \pm 0.1 K on frost-point temperature (T_{fp}) for range $T_{fp} > -95$ °C, corresponding to < 2 % in H ₂ O mixing ratio	In situ	Participant

* During AquaVIT-4, there was additional uncertainty (up to \pm 0.2 ppm H₂O at low p_{AIDA}) due to the extractive configuration (see Appendix A3).

approximately 1–30 m, depending on the aircraft. The DLH instrument that was used during AquaVIT-4 (DLH-WB) is the one which has flown on the NASA WB-57F aircraft during several campaigns since 2008, reaching approximately 20 km altitude in flights lasting up to 6 h (e.g., Rollins et al., 2014).

The transceiver in the DLH-WB is mounted inside an airfoil-shaped fin which is mounted beneath the aircraft wing, and the retroreflective film is typically located on either a thin antenna-like fin mounted beneath an instrument pod or on an engine nacelle on the same wing as the transceiver. Optical paths on this aircraft ranged from approximately 13 to 18 m. For AquaVIT-4, the DLH-WB instrument housing (which contains the laser itself and all data acquisition and control, as well as the transceiver) was mounted outside the chamber in the cold zone, and the optical beam was passed through a custom-antireflection-coated plane-parallel window into and out of the chamber. The retroreflective film was mounted on the inside of a window blank on the opposite side of the chamber, resulting in a two-pass optical

path in the chamber of about 9.41 m. The short path between the instrument transceiver window and the facility window was covered by a custom housing and purged continuously with synthetic ultra-dry air. External heaters were added to the instrument housing to maintain a minimum temperature of approximately -20 °C while the instrument was unpowered during the overnight hours. During testing hours, those heaters remained on, but internal temperatures were maintained via the same heaters and control system which operate during flight.

To measure water vapor, the DLH laser is tuned to one of three spectral absorption lines near 1.395 μ m. These three lines have line strengths which each differ by nearly an order of magnitude, allowing the instrument to measure water vapor in the atmosphere over its entire dynamic range. In flight, the DLH control software selects the appropriate absorption line for the conditions and switches automatically between them to maintain good instrument performance. During AquaVIT-4, due to the unusual circumstances of the fa-

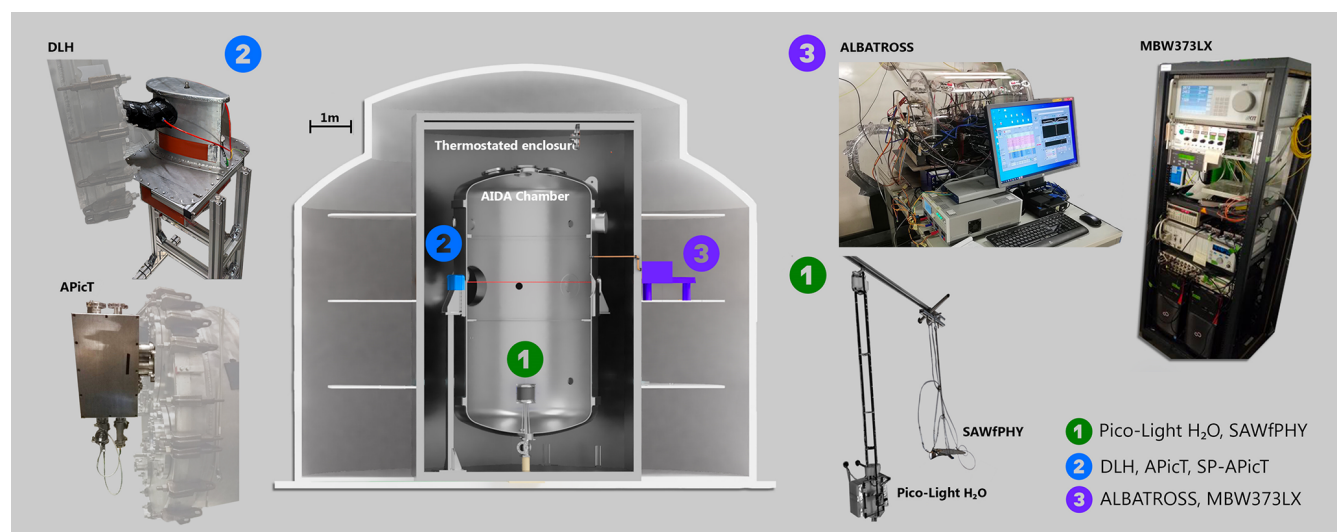


Figure 1. Schematic of the experimental setup used within the AquaVIT-4 intercomparison campaign.

cility operation, operating modes were adjusted manually, and for all reported data, only the strongest line was used.

DLH uses line-locked, multi-harmonic wavelength modulation spectroscopy to achieve high accuracy, high precision, and fast temporal response. For AquaVIT-4, only the second harmonic was used to convert signal to water vapor mixing ratio. Because of the dependence of absorption signal on temperature and pressure, both in flight and in ground-based facilities, conversion of DLH data to water vapor mixing ratio requires additional information on those parameters as well as the installed optical path length. For AquaVIT-4, the temperature and pressure data were provided by the AIDA facility operators through a network interface.

3.3 Pico-Light H₂O tunable-diode laser hygrometer

Pico-Light H₂O is a mid-infrared lightweight tunable-diode laser hygrometer, probing water vapor at 2.63 μm . The Pico-Light instrument was primarily developed for sounding of the upper troposphere and stratosphere. It relies on mid-infrared direct absorption spectroscopy. The beam of a 2.63 μm antimonide laser diode is propagated in the open atmosphere over a 1 m distance; absorption spectra are thereby recorded in situ at 10 ms intervals by ramping the driving laser current. The water vapor mixing ratios are retrieved from the in situ absorption spectra using a molecular model (here Voigt profile) in conjunction with in situ atmospheric pressure and temperature measurements. The absolute pressure is measured by an absolute pressure transducer (precision 0.05 % full scale, absolute uncertainty 0.5 hPa; model PPT1, Honeywell, USA) and the air temperature is measured using two fast-response temperature sensors (Sippican, USA) with an uncertainty of 0.2 K root mean square and a resolution of 0.1 K. Their uncertainty was improved by an intercomparison program with the World Meteorological Or-

ganization (WMO) (Nash et al., 2011). One sensor is located at each end of the optical cell. The enhanced electronics are both smaller and more energy-efficient compared with those employed in previous Pico-SDLA. This decrease in power consumption and shorter flight duration have contributed to a significant one-third reduction in the energy budget, now standing at just 3.5 Wh.

Pico-Light H₂O was compared in flight with the NOAA FPH during the AsA 2022 balloon campaign from the CNES Aire-sur-l'Adour (France) balloon launch facility (Ghysels et al., 2024).

3.4 SAWfPHY acoustic wave frost-point hygrometer

SAWfPHY is a recently developed low-power (3W), lightweight instrument (3 kg) aimed at performing water vapor measurements on board long-duration balloon flights in the lower stratosphere. SAWfPHY has already performed several month-long flights in the tropical lower stratosphere, in the framework of the Strateole-2 project. SAWfPHY is a frost-point hygrometer. Yet, instead of standard frost-point hygrometers that use optical methods to detect frost on a mirror, the sensing surface of SAWfPHY is a surface acoustic wave (SAW) resonator. The sensor, which is cooled by a Peltier thermoelectric device, is enclosed in a stainless-steel chamber, into which air is pumped from the outside. The resonator properties (peak frequency and factor of quality) are modified by the ice deposit on the substrate. The control loop of the instrument is thus designed to maintain a constant and detectable amount of ice on the sensor, at which point the resonator temperature is equal to the frost-point temperature. The resonator temperature is measured by a bead thermistor located close to it, and the saturation vapor pressure over ice (Murphy and Koop, 2005) is used to convert the measured

frost-point temperature into water vapor partial pressure (and mixing ratio).

During the AquaVIT-4 campaign, SAWfPHY's sensing chamber was located in the main AIDA vessel, next to the Pico-Light H₂O instrument. On the other hand, the instrument electronics were located outside of the vessel, in the laboratory. The airflow inside the sensing chamber was ensured during AquaVIT-4 by connecting the chamber to the vacuum line of AIDA through a mass-flow controller. During balloon flights, the airflow is ensured by a pump working at atmospheric pressure. The instrument performed nominally during the 2 campaign weeks, except for 2 d corresponding to the coldest AIDA temperature set points (day 4 of the open intercomparison with $T_{\text{AIDA}} \sim 194$ K and day 3 of the blind intercomparison with $T_{\text{AIDA}} \sim 190$ K). During those periods, a short circuit in the cables or connections between the sensing chamber and the electronics prevented any measurement (see Appendix A6 for further details). Note that in the balloon-borne configuration of the instrument, measurements have been performed at even colder temperatures than those experienced in AIDA.

3.5 Reference instruments

3.5.1 APicT and SP-APicT tunable-diode laser spectrometers

Two fiber-coupled tunable-diode laser hygrometers (APicT and SP-APicT) measure the water vapor concentration at the AIDA chamber based on its absorption at 1370 nm. Both instruments are designed to selectively detect interstitial water vapor inside clouds and to continuously determine the absolute water vapor mixing ratio inside the AIDA chamber (Ebert et al., 2005; Skrotzki, 2012; Skrotzki et al., 2013; Fahey et al., 2014; Sarkozy et al., 2020; Lamb et al., 2023). While APicT is connected to White-cell optics, allowing for a variable optical path between typically 23–99 m (200 m optionally), SP-APicT has an optical path length of only about 4 m, passing once across the chamber diameter. For the in situ measurement of water vapor concentration and partial pressure, the time resolution is approximately 1 s and the accuracy is given at ± 5 %. The total water content is retrieved by extractive sampling of AIDA gas via a heated stainless-steel line in which ice and water droplets evaporate. To this line, the frost-point mirror hygrometer MBW-373LX (see below) is connected. From the difference of total water and water vapor measurements, the condensed or cloud water content within AIDA can be derived. The water partial pressure obtained by the TDL instruments can be converted into an ice saturation ratio or relative humidity using the water vapor saturation pressure with respect to the AIDA gas temperature (Murphy and Koop, 2005). The accuracy of the retrieval of the relative humidity is therefore determined not only by the accuracy of the water vapor pressure but also by the uncertainty of the gas temperature. The AIDA mean gas tempera-

ture is determined by averaging over a representative number of 24 calibrated thermocouples distributed over the chamber volume in horizontal and vertical chains.

3.5.2 MBW-373LX dew-point mirror hygrometer

The MBW-373LX is a chilled-mirror frost-point hygrometer from MBW Calibration AG, Switzerland (now Process-Insights Inc.) that is used regularly in the AIDA facility. The unit has a frost-point accuracy of ± 0.1 K traceable to calibration standards. The MBW-373LX instrument is located outside the AIDA chamber. It is connected to the chamber via 10 mm stainless-steel tubes extending 40 cm into the chamber volume. With a three-way valve either an inlet located at level 2 or at level 3 of the AIDA chamber can be selected. Both sampling tubes are heated to 30 °C from the inlet to outside of the cold box. For this study only the direct connection to the instrument on level 2 of the AIDA chamber was used with a total volume of 0.4 L. Typical flow rates through the instrument are 1.0 SLM at a total chamber pressure of 1000 hPa, decreasing to about 0.3 SLM at a pressure of 100 hPa. For lower pressures, the smaller flow rate leads to a slower time response of the instrument. Lower water vapor concentrations also typically result in a slower time response of the frost-point mirror of the order of several minutes, since it requires more time to build up a detectable frost layer. Reference measurements at a water vapor pressure corresponding to saturation at 213 K showed a time resolution of 30 s of the instrument.

4 Experiments and data analysis

The AquaVIT-4 campaign was divided into two phases: an “open intercomparison”, carried out between 29 March and 1 April 2022, and a “blind intercomparison”, carried out between 4–7 April 2022. Each phase comprised 4 experimental days, with each day consisting of 7–9 h of measurements in the AIDA chamber.

During the open intercomparison, the temperature, pressure, and H₂O content of the AIDA chamber were defined jointly by the instrument team members, and “quick looks” (i.e., preliminary evaluations) of the data by all instruments could be freely exchanged between the groups. This phase provided a valuable first intercomparison dataset, while allowing optimization of the operation of the AIDA chamber and the design of the experiments.

During the blind intercomparison, the conditions of the AIDA chamber were determined by an independent board of referees, not affiliated with any participating instrument team and unknown to the participants. The referee board consisted of the following members: Masatomo Fujiwara (Hokkaido University, Japan), Karen Rosenlof (NOAA, USA), and Ottmar Möhler (KIT, Germany).

Table 2. Simulated conditions in the AIDA chamber during each day of the intercomparison (open, blind) in terms of temperature (T_{AIDA} , mean \pm standard deviation), pressure (p_{AIDA} , min–max range), H₂O mixing ratio (measured by APicT, min–max range), and number of different set points (N_{SP} , i.e., static intervals).

Date	Type	Abbrev.	T_{AIDA} [K]	p_{AIDA} [hPa]	H ₂ O APicT [ppm]	N_{SP}
2022-03-29	Open	OD1	226 \pm 2	120–500	30–200	7
2022-03-30	Open	OD2	244 \pm 3	100–600	100–530	8
2022-03-31	Open	OD3	209 \pm 3	20–325	3–20	6
2022-04-01	Open	OD4	194 \pm 2	70–180	0.5–2	5
2022-04-04	Blind	BD1	220 \pm 3	20–250	1–80	10
2022-04-05	Blind	BD2	204 \pm 2	20–150	1.5–20	10
2022-04-06	Blind	BD3	190 \pm 1	70–100	0.5–3	7
2022-04-07	Blind	BD4	234 \pm 3	50–400	25–400	13

The conditions were defined by the referee board based on the typical ranges of H₂O mixing ratio in the UTLS available in the literature and on the operational constraints of the AIDA chamber. Then, each instrument team reported their final data independently by submitting them directly to the referee board, without having access to either the reference instrument measurements or to those of other instruments. Finally, the referee board created time series plots of all the measurements (similar to Fig. 4) and disclosed the data.

An exception to the blind intercomparison protocol was made after the disclosure of the results to allow the revision of a minor portion of the blind intercomparison datasets by two participating instruments (Pico-Light H₂O and SAWF-PHY). The reasons for this exception are documented in detail in Appendix A5 and A6.

4.1 Simulated conditions

During each day of measurements, the temperature of the AIDA chamber (T_{AIDA}) was kept mostly constant, while pressure (p_{AIDA}) and H₂O mixing ratio were varied in steps, aiming to simulate the conditions of a given layer of the atmosphere (from the mid-troposphere to the lower stratosphere). Changes in p_{AIDA} were achieved by the addition/removal of dry synthetic air (22.5 % O₂ in N₂, H₂O < 3 ppm) from/to the chamber, while changes in H₂O mixing ratio were achieved by injecting a given amount of pure H₂O into the chamber, either before the start or during the course of each experiment. Overnight between the experiments, the chamber was evacuated to less than 0.01 hPa pressure.

The ranges of T_{AIDA} , p_{AIDA} , and H₂O mixing ratio (according to the APicT measurements) established during each day of both the open and blind intercomparison are summarized in Table 2. The first 2 d of the open intercomparison (OD1, OD2) focused on simulating middle- to upper-tropospheric conditions, with T_{AIDA} between 226–244 K and high H₂O content (\sim 30–500 ppm). Then, the chamber was cooled down to simulate UTLS (209 K, OD3) and tropical tropopause (194 K, OD4) conditions, with their associated low H₂O content (< 20 ppm). Day 1 of the blind intercom-

parison (BD1) spans a wide range of pressures (20–250 hPa) and H₂O mixing ratios (1–80 ppm) at around 220 K, simulating both upper-tropospheric and lower-stratospheric conditions (separately). Then, T_{AIDA} was reduced to UTLS (204 K, 1.5–20 ppm H₂O, BD2) and tropical tropopause (190 K, 0.5–3 ppm H₂O, BD3) conditions. Finally, on BD4 the chamber was warmed up to 234 K to simulate mid- and upper-tropospheric conditions (with up to 400 ppm H₂O).

Figure 2 displays the distributions of the mean H₂O mixing ratio (measured by APicT) against p_{AIDA} and T_{AIDA} (color-coded) of all the measured static intervals (“set points”), overlaid with two vertical profiles of H₂O mixing ratio in the atmosphere. The atmospheric profiles have been measured by the CFH during recent field campaigns and correspond to moist, tropical summer conditions (dashed gray line) and dry, midlatitude winter conditions (solid gray line). Open intercomparison and blind intercomparison set points are indicated by empty and filled dots, respectively. Note that the selection of the set point intervals is described in Sect. 4.3.

Figure 2 shows that the simulated conditions in the AIDA chamber during AquaVIT-4 cover the expected range of variability of H₂O in the UTLS well, up to pressures of \sim 20 hPa (corresponding to approximately 28 km altitude) and for different latitudes and seasons. Furthermore, H₂O mixing ratios that are below those typically observed in the atmosphere (< 2 ppm) were also investigated in both the open and blind intercomparison. These measurements represent extremely dry conditions that can be associated with tropical deep convection (typhoon) events, for example during the overpass of the Pico-SDLA instrument over the typhoon Raï during the Strateole 2 campaign, with mixing ratios of 1.5–2 ppm H₂O (Carbone et al., 2025). Although rarely found in the atmosphere (e.g., Inai et al., 2012; Brunamonti et al., 2018, 2019), measuring mixing ratios below 2 ppm H₂O is useful to assess the detection limits of the different instruments.

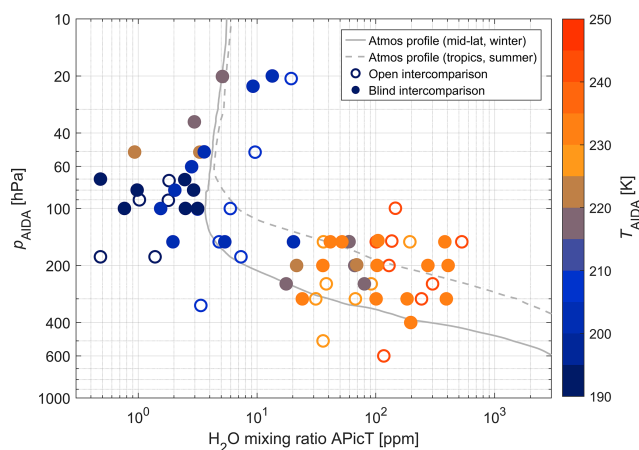


Figure 2. Scatter plot of pressure (p_{AIDA}) vs. H_2O mixing ratio (according to APicT measurements) and temperature (T_{AIDA} , color-coded) measured during all static intervals (i.e., set point) of the intercomparison, overlaid with two atmospheric profiles of UTLS H_2O . The profiles correspond to tropical summer conditions (dashed gray line: Brunamonti et al., 2018) and midlatitude winter conditions (solid gray line: Graf et al., 2021) and were smoothed by a ± 1 km moving average. Open intercomparison and blind intercomparison set points are indicated by open and filled circles, respectively.

4.2 Measurement overview

Figures 3–4 show the time series of the H_2O mixing ratio measured by all instruments, along with pressure and temperature of the AIDA chamber, for each day of the open (Fig. 3) and blind (Fig. 4) intercomparison. As already mentioned, each day of experiment was performed at constant T_{AIDA} , while the H_2O mixing ratio varied depending on the amount of water added directly to the chamber at the beginning of each day and on subsequent changes in pressure. Each combination of H_2O and p_{AIDA} was held constant for about 30–60 min, for a total of 5–13 atmospherically relevant static condition sets measured during each day. The transient temperature changes shown in Figs. 3–4 are the adiabatic response to rapid addition or removal of air from the chamber, while the walls and enclosure remain at constant temperature.

While generally the H_2O mixing ratio values were kept below the ice saturation level, ice-saturated and even supersaturated conditions were also generated in the AIDA chamber at a few instances by forming ice clouds. Particularly, this can be seen in OD4 (Fig. 3f, time ~ 6 –7 h), BD2 (Fig. 4b, time ~ 7 h), and BD3 (Fig. 4f, time ~ 9 –10 h). During these conditions, due to the evaporation of the ice crystals contained in the AIDA chamber during their transport inside the heated sampling tube, the extractive instruments (ALBATROSS and MBW373LX) measured the total (i.e., sum of gas and condensed phase) H_2O content of the chamber, whereas non-extractive instruments (all oth-

ers) measured the gas-phase H_2O only. These measurements are particularly valuable since, assuming the ice cloud is dense enough to sustain a constant relative humidity over ice (RH_{ice}) of 100 %, they provide an intrinsic reference for the gas-phase (non-extractive) instruments, corresponding to the ice-saturated H_2O mixing ratio, which can be calculated based on the p_{AIDA} and T_{AIDA} measurements. The in-cloud interval measured during BD2 is analyzed in detail in this respect in Sect. 5.1.

The measurements of the extractive and non-extractive instruments also differ systematically due to adsorption/desorption effects of H_2O , particularly the desorption of H_2O molecules from the inner walls of the sampling tube (especially at low pressure), increasing the H_2O mixing ratio in the sample gas and causing a memory effect in the system. Since the rate of adsorption/desorption has a complex dependency on pressure, water content, and sampling time (e.g., note that the difference between extractive and non-extractive instruments is larger in OD1 compared to OD3 at similar pressure conditions: Fig. 4a, d), these effects are particularly difficult to quantify. For this reason, we decided to separately define reference values for extractive and non-extractive instruments (see Sect. 4.4).

Adsorption/desorption on the chamber walls can also affect the H_2O mixing ratio inside the AIDA chamber. An example of this can be seen in OD3 (Fig. 2e–g, time ~ 3 –9 h), when the H_2O mixing ratio in the chamber increases from ~ 3 ppm to ~ 20 ppm upon a decrease in p_{AIDA} from 325 to 20 hPa. Since no additional H_2O was added to the chamber during this interval and the mixing ratio should remain constant as air is pumped from the chamber, this increase must be due to the desorption of H_2O molecules from the inner walls of the chamber (or other internal components).

4.3 Statistical intercomparison

To quantify the differences between each participating instruments and their corresponding reference, a series of data intervals that provided nearly constant H_2O mixing ratio, p_{AIDA} , and T_{AIDA} (hereafter “set points”) were selected for each day. Set point intervals, with a duration of 10 min each, were defined individually based on the analysis of the measured time series and typically placed before a change in pressure or the injection of H_2O in the AIDA chamber occurred. Segments with static conditions that are irrelevant for the atmosphere (e.g., low H_2O mixing ratios at high pressure, and vice versa) were excluded from the statistical analysis. In total, 66 atmospherically relevant set points could be identified during the open (26) and blind (40) intercomparison, which are shown as gray shaded intervals in Figs. 3–4.

The data from all instruments are expressed as H_2O mixing ratio (or molar fraction) in units of $\mu\text{mol mol}^{-1}$ (i.e., parts per million, ppm) and submitted with a raw time resolution of approximately ~ 0.3 s (Pico-Light), ~ 0.7 s (APicT, SP-APicT), ~ 0.9 s (ALBATROSS), and ~ 1 s (DLH, SAWf-

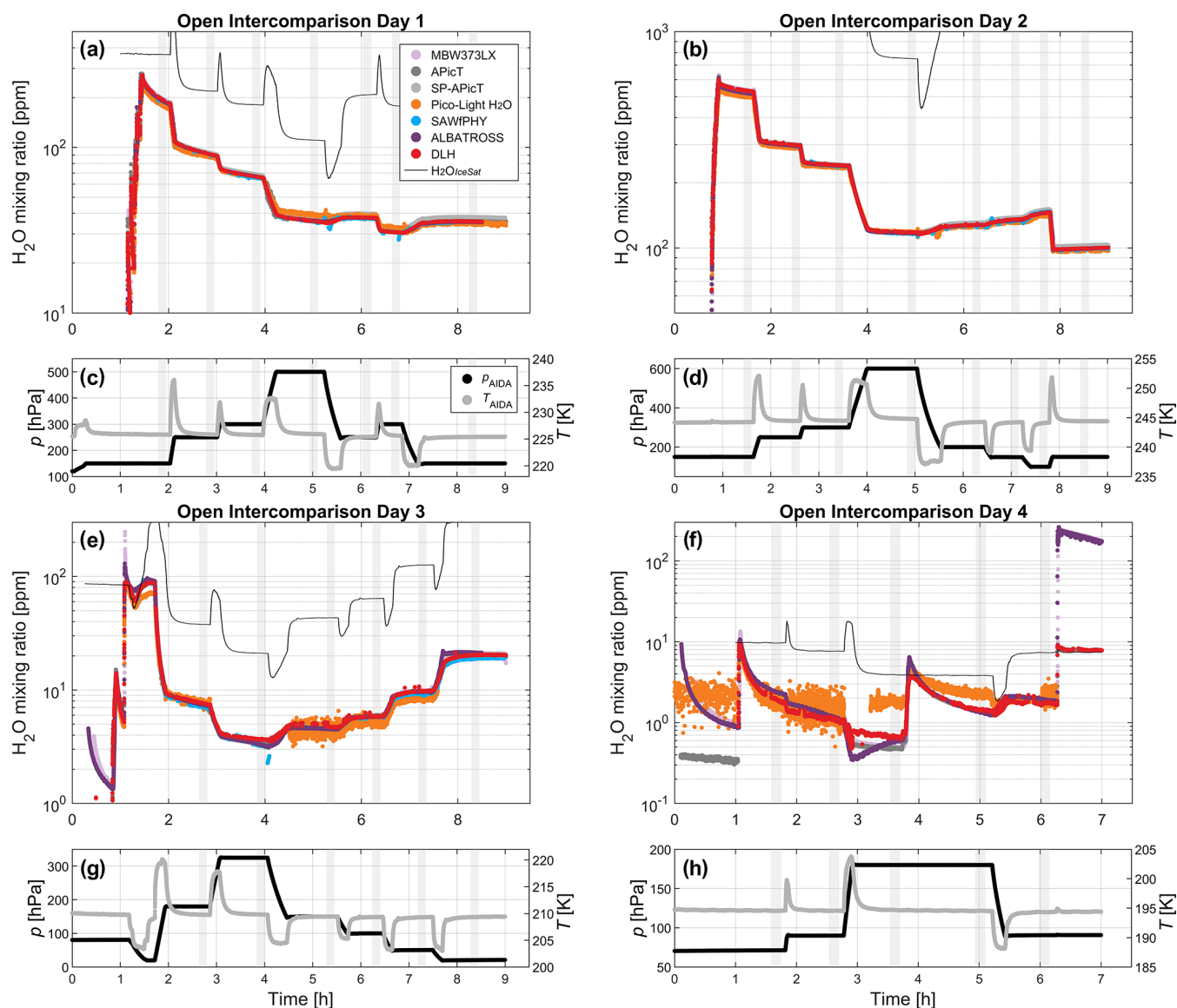


Figure 3. Time series of H_2O mixing ratio measured by all instruments (a–b, e–f), namely MBW373LX (pink), APicT (dark gray), SP-APicT (light gray), Pico-Light (orange), SAWfPHY (blue), ALBATROSS (purple), and DLH (red), along with AIDA chamber pressure (p_{AIDA}) and temperature (T_{AIDA}) (c–d, g–h) for each day of the open intercomparison phase of the campaign. All data shown here are averaged to a uniform integration time of 2 s. The static intervals selected for the statistical comparison (i.e., set points) are identified by the gray shaded intervals (duration 10 min each). Note that, for consistency, the color coding applied here to the different instruments is used consistently in all the following figures. The initial phases, especially of the experiments with lower water mixing ratios, were intended to give the sampling lines time to dry. The solid black line in (a)–(b) and (e)–(f) shows the ice-saturated H_2O mixing ratio ($\text{H}_2\text{O}_{\text{IceSat}}$) calculated from p_{AIDA} and T_{AIDA} (see Sect. 5.3).

PHY, MBW373LX). For the statistical comparison, the entire dataset is first averaged to an integration time of 2 s, and the relative differences ($\Delta\text{H}_2\text{O}$) between each instrument and reference are calculated for each time step. Note that the choice of reference instrument to be associated with each category of instrument (extractive vs. non-extractive sampling) and H_2O mixing ratio range is discussed in the next section. Then, for each set point, the mean relative difference

and standard deviation are calculated as the mean and standard deviation of $\Delta\text{H}_2\text{O}$ over the corresponding time period. Finally, to quantify the results in terms of H_2O mixing ratio range, the mean relative differences are further averaged over four ensembles of set points, defined by a given condition in the average H_2O mixing ratio of the reference instrument (e.g., $\text{H}_2\text{O} < 2$ ppm). For each range, the mean relative deviation (μ) and standard deviation (σ) are calculated as the

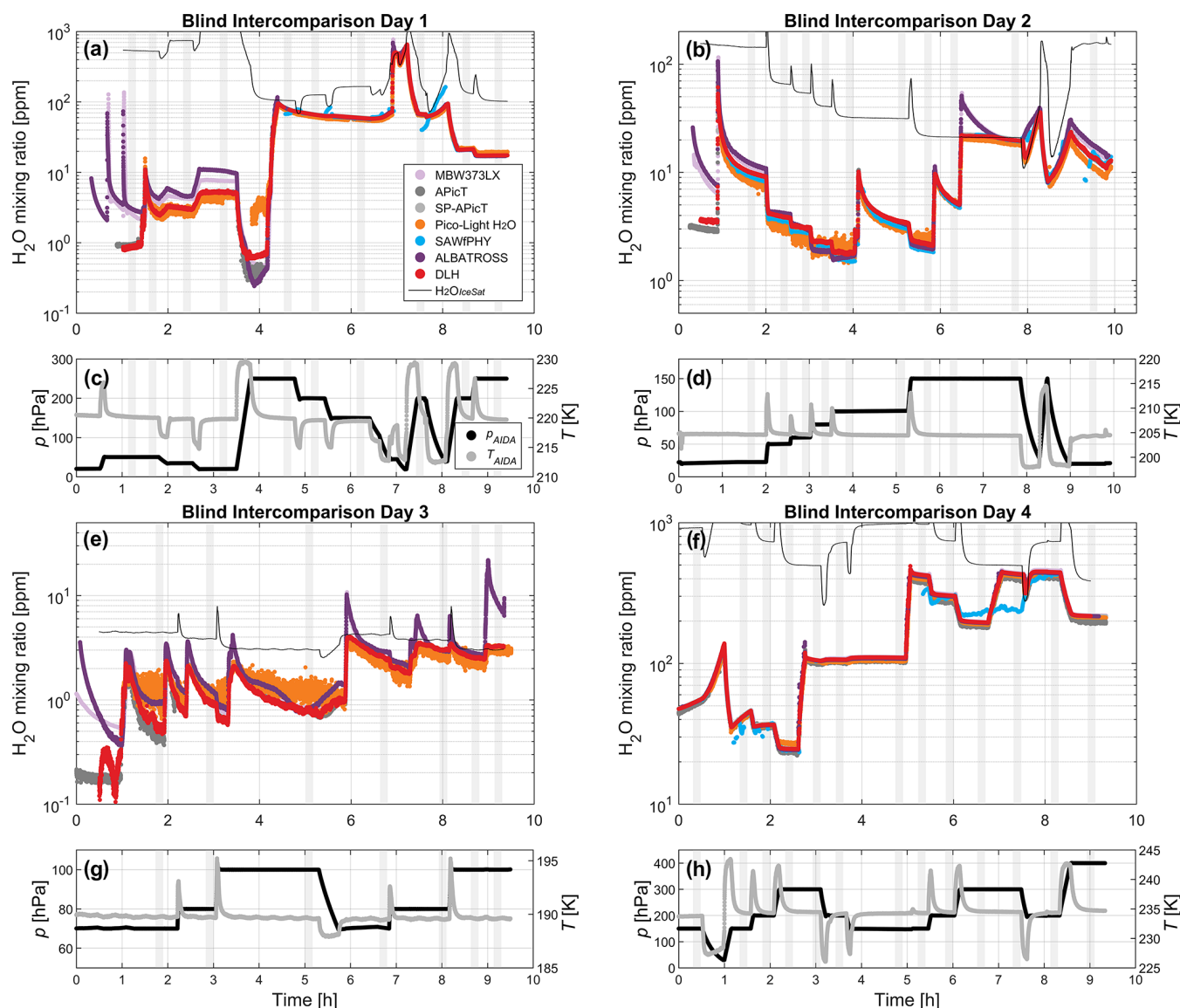


Figure 4. Same as Fig. 3 for the blind intercomparison phase of the campaign.

mean and standard deviation over all set points belonging to that range.

The results of the statistical comparison are discussed in Sect. 5.1. The equations used for the data analysis, as well as a list of all set points measured during the campaign, can be found in the Supplement.

4.4 Reference instruments

Before evaluating the results of the participating hygrometers, the differences between the three reference instruments are systematically investigated with the aim of defining the most appropriate reference instrument for each participating instrument, depending on sampling method (extractive vs. in situ) and H_2O mixing ratio range.

In AquaVIT-1 (Fahey et al., 2014), in the absence of an accepted reference for establishing the absolute accuracy of the instruments, the reference value for each static interval was taken as the ensemble mean of a “core” subset of instruments, showing deviation within $\pm 10\%$ from such a reference value at all conditions. It is relevant to note here that the “core” subset of instruments of AquaVIT-1 included both internal and external instruments, and the MBW373LX was not included in this subset. This was due to the fact that the MBW373LX flow rate dropped below ~ 0.3 SLM whenever the AIDA pressure was lower than 100 hPa, leading to a very slow response time of the instrument and memory effect in the sampling line and, thus, a systematic deviation with respect to the non-extractive instruments (Fahey et al., 2014).

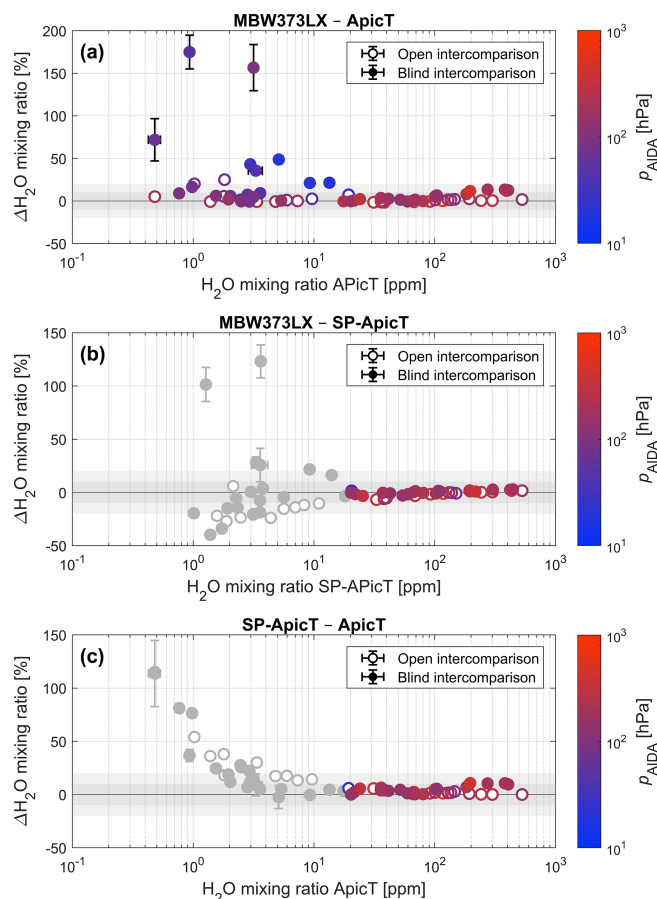


Figure 5. Scatter plots of the mean relative difference between the three reference instruments, namely MBW373LX – APiCT (a), MBW373LX – SP-APiCT (b), and SP-APiCT – APiCT (c), as a function of the measured H_2O mixing ratio, calculated for all set points of the open (open circles) and blind (filled circles) intercomparison and color-coded with AIDA pressure (p_{AIDA}). The set points associated with H_2O mixing ratios lower than 20 ppm have been shaded in the two lower panels because of the limitations of the SP-APiCT instrument at these low values (see Sect. 4.4).

In our case, given the presence of a single external participant (ALBATROSS), which shares the same sampling line with the MBW373LX and has a comparable flow rate (see Sect. 3), we can argue that the two instruments are subject to the same artifacts and use the MBW373LX data as a reference for ALBATROSS. Therefore, two reference values are defined for each set point: one “internal” reference (Ref_{Int}), applied to the in situ instruments (Pico-Light H_2O , SAWPHY, DLH), and one “external” reference (Ref_{Ext}), applied to the extractive instrument (ALBATROSS).

Figure 5 shows the scatter plots of the mean relative difference between the three reference instruments, namely MBW373LX – APiCT (panel a), MBW373LX – SP-APiCT (b), and SP-APiCT – APiCT (c), as a function of the measured H_2O mixing ratio for all set points of the open (white

dots) and blind (filled dots) intercomparison color-coded with p_{AIDA} .

Three main effects influence the behavior of the reference instruments: (i) slower time response due to required drying of the sampling tube (surface effects), leading to a systematic high bias of the extractive measurements with respect to the internal ones (Fig. 5a–b); (ii) longer times required to build up a detectable frost layer on the MBW373LX mirror at low H_2O mixing ratios; and (iii) additional internal water absorption affecting the retrievals of the short-path SP-APiCT, caused by water vapor in the sealed laser compartment, leading to a systematic moist bias of SP-APiCT with respect to APiCT at low H_2O mixing ratios (Fig. 5c, gray dots).

Figure 5a shows that larger differences between extractive and in situ measurements tend to be associated with lower pressures in the AIDA chamber (see range of 5–10 ppm H_2O), which is consistent with the pressure-dependent desorption of H_2O molecules in the sampling line (i). However, no direct correlation can be inferred due to the involved memory effects. The slow response time of MBW373LX due to the build-up of the frost layer (ii) is compensated for by selecting static intervals with nearly constant H_2O mixing ratios.

The moist bias due to the absorption of water vapor in the hermetically sealed laser compartment (iii) is a well-known feature of some DFB-TDL systems, like SP-APiCT, coupled by fibers to a measurement volume as at the AIDA chamber (Buchholz and Ebert, 2014). This additional absorption signal leads to a larger bias for the measurement with a shorter optical path length in the measurement volume. Therefore, SP-APiCT should be used only for H_2O mixing ratios > 100 ppm (Skrotzki, 2012; this work) or be corrected for the additional absorption (e.g., by quantifying the additional absorption with measurements at lower total pressure in the AIDA chamber).

Consequently, the internal and external reference values for each static interval are defined according to Eqs. (1)–(2). Specifically, Ref_{Int} is defined as equal to the APiCT retrieval for all set points with mean H_2O mixing ratio lower than 100 ppm and equal to the SP-APiCT retrieval for all set points with mean H_2O mixing ratio higher than 100 ppm, while Ref_{Ext} is equal to the MBW373LX retrieval for all set points.

$$\text{Ref}_{\text{Int}} = \begin{cases} \text{APiCT}, & \text{if } \text{H}_2\text{O}_{\text{APiCT}} < 100 \text{ ppm} \\ \text{SP-APiCT}, & \text{if } \text{H}_2\text{O}_{\text{APiCT}} > 100 \text{ ppm} \end{cases} \quad (1)$$

$$\text{Ref}_{\text{Ext}} = \text{MBW373LX} \quad (2)$$

The uncertainty of the reference measurements is defined by the uncertainty of the individual reference instruments, given in Table 1. A comparison of the internal reference measurements with the ice-saturated H_2O mixing ratio during experimental phases with dense ice clouds is discussed in Sect. 5.2 and demonstrates the quality of the reference data.

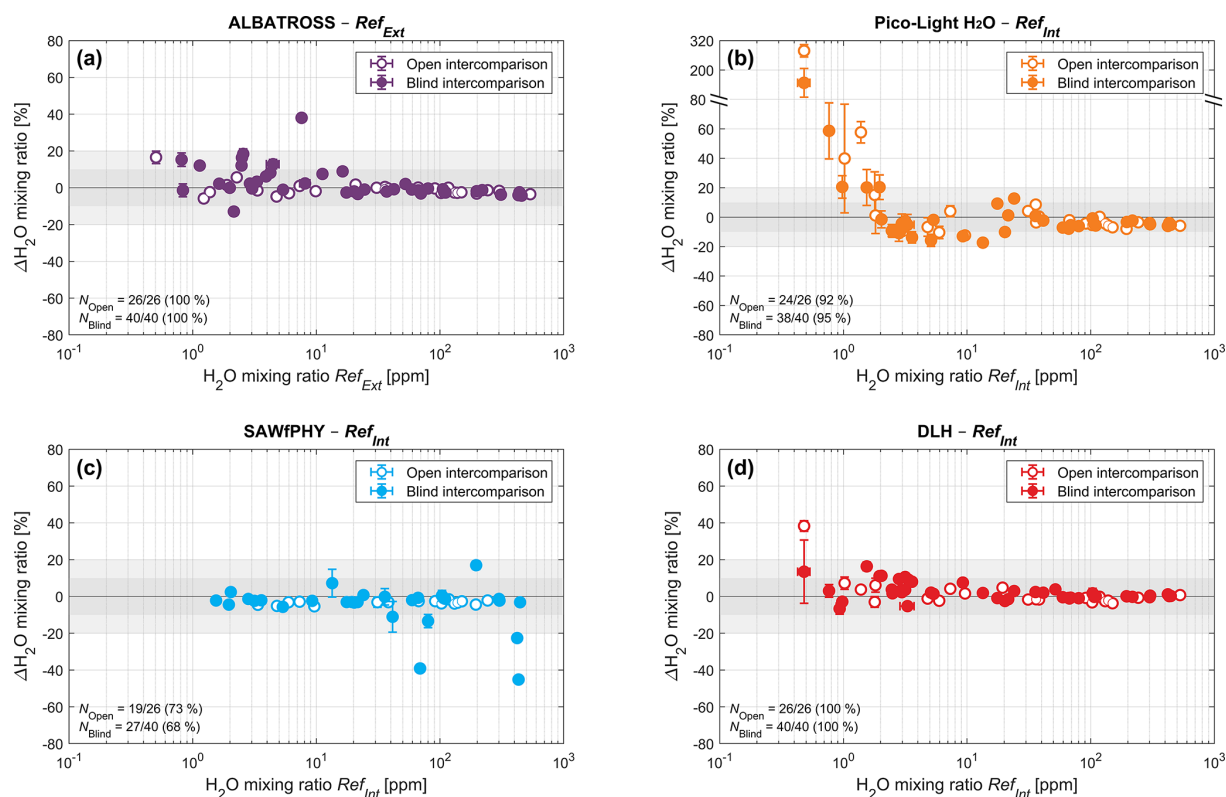


Figure 6. Scatter plots of the mean relative difference ($\Delta\text{H}_2\text{O}$) of each instrument with respect to its reference dataset, namely ALBATROSS – Ref_{Ext} (a), Pico-Light – Ref_{Int} (b), SAWfPHY – Ref_{Int} (b), and DLH – Ref_{Int} (d), calculated for all set points of the open (open circles) and blind (filled circles) intercomparison. Vertical error bars show the standard deviation range of the difference within each set point, while horizontal error bars show the standard deviation range of the reference H_2O mixing ratio.

5 Result

Here we analyze the performance of the instruments in terms of accuracy with respect to the reference measurements (Sect. 5.1) as well as precision (Sect. 5.2). A detailed analysis of an in-cloud measurement interval at ice saturation, providing an independent internal reference, is presented in Sect. 5.3.

5.1 Accuracy

The results of the statistical comparison are presented in Fig. 6 and summarized in Table 3. Figure 6 shows the scatter plots of the mean relative difference (μ) of each instrument with respect to its reference dataset, namely ALBATROSS – Ref_{Ext} (panel a), Pico-Light H_2O – Ref_{Int} (b), SAWfPHY – Ref_{Int} (b), and DLH – Ref_{Int} (d), calculated for all set points of both the open and blind intercomparison. Vertical error bars show the $\pm 1\sigma$ range of standard deviation of the difference (calculated according to Eq. 3), while horizontal error bars show the standard deviation range of the reference H_2O mixing ratio. Table 3 shows the mean values of $\mu \pm \sigma$ for each instrument and set point of the blind intercomparison, calculated in five ranges of H_2O

mixing ratio, namely $\text{H}_2\text{O}_{\text{Ref}} < 2$ ppm, $\text{H}_2\text{O}_{\text{Ref}} = 2\text{--}10$ ppm, $\text{H}_2\text{O}_{\text{Ref}} = 10\text{--}100$ ppm, and $\text{H}_2\text{O}_{\text{Ref}} > 100$ ppm, as well as all data together, along with the number of set points measured by each instrument in each range (N_{SP}). Note that the range of each set point is assigned for each participating instrument depending on the mean H_2O mixing ratio of the reference instruments associated with that participant (i.e., Ref_{Ext} for ALBATROSS and Ref_{Int} for all other instruments).

$\text{H}_2\text{O} < 100$ ppm: at higher H_2O mixing ratios, the agreement between participants and reference instruments is generally very good. Most instruments (ALBATROSS, DLH, Pico-Light H_2O) achieve a mean deviation smaller than $\pm 4\%$ with respect to the reference, with standard deviations of 1% – 2% (see Table 3), and all measured set points within $\pm 8\%$. The only exception is SAWfPHY, showing larger discrepancies ($> 10\%$) for three of the measured set points in this range and a mean deviation of $-7 \pm 19\%$ (Table 3). This is due to the fact that during the second half of BD4, the AIDA temperature set point was higher than -40°C (see Fig. 4h). Therefore, uncertainties in the phase condensate on SAWfPHY's sensor caused a biased estimation of the H_2O partial pressure (see more details in Appendix A6).

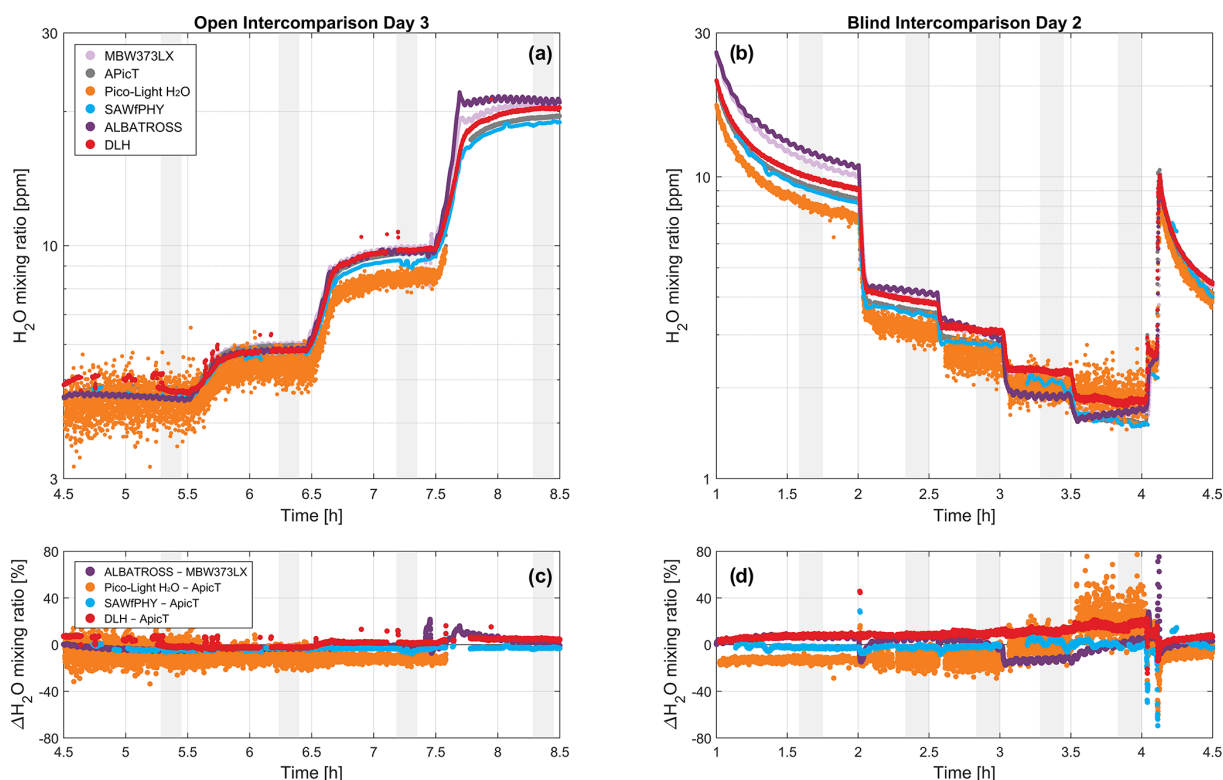


Figure 7. Detail of the time series of two selected measuring intervals in the range 2–10 ppm H₂O, namely from the OD2 (a, c) and BD2 (b, d). (a–b) H₂O mixing ratio measured by all instruments (same color coding as in Figs. 3–4) at integration time 2 s. (c–d) Relative difference (in percent units) between each instrument and its corresponding reference. In all panels, set point intervals are highlighted by the gray shaded areas.

H₂O = 10–100 ppm: in this range, all instruments obtain good agreement with the reference measurements. ALBATROSS and DLH achieve a mean accuracy of $0 \pm 4\%$ and $0 \pm 2\%$, respectively, and all set points within a deviation of $\pm 9\%$ (ALBATROSS) and $\pm 4\%$ (DLH) with respect to their reference. For Pico-Light H₂O, the mean accuracy is $-3 \pm 9\%$ with all set points within $\pm 18\%$, while SAWfPHY achieves a mean accuracy of $-6 \pm 12\%$ and deviations smaller than $\pm 20\%$ for all except one set point, which is again due to the dry bias observed in BD4.

H₂O = 2–10 ppm: for H₂O mixing ratios between 2–10 ppm, the mean discrepancy of all instruments stays within $\pm 8\%$, whereas the relative standard deviations tend to increase due to the reduced H₂O content. ALBATROSS and DLH tend to show a slight overestimation of the reference H₂O mixing ratios, with mean accuracies of $8 \pm 12\%$ and $5 \pm 5\%$, respectively, over all set points of the blind intercomparison. Pico-Light H₂O and SAWfPHY show a slight underestimation of the reference measurements, with mean deviations of $-8 \pm 5\%$ and $-2 \pm 3\%$, respectively (Table 3). The ALBATROSS standard deviation is strongly influenced by a single set point with a deviation of $\sim 40\%$ measured in BD1 at $p_{AIDA} \sim 20$ hPa (see Fig. 4a). For SAWfPHY, only less than half (6 out of 13) of the set points in this range were

measured due to the connection issues that occurred in BD3 (see Sect. 3.2).

Figure 7 shows a detail of the time series of two selected measuring intervals in the range 2–10 ppm H₂O, namely OD3 (panel a) and OD2 (b), along with the relative difference between each instrument and its corresponding reference (c–d). One noteworthy feature shown here is the small-scale fluctuations in H₂O (peak-to-peak amplitude ~ 0.1 ppm) observed in the extractive instruments ALBATROSS and MBW373LX. These fluctuations are a measurement artifact due to the heating controller of the sampling line, shared by both instruments, which modulates the temperature (hence the H₂O mixing ratio via temperature-induced adsorption/desorption effects on the inner walls of the sampling line) with a period of about 3 min. This artifact is not corrected in the statistical comparison, and hence the fluctuations appear in the difference between the two instruments as well (Fig. 7c–d). The slight phase offset between the two retrievals is likely due to the different flow rate/response time of the two instruments. The fluctuations are instead corrected by a sinusoidal fit for the precision analysis (see next section).

The Pico-Light H₂O measurements depict an increased dispersion when the pressure increases with a

decreasing mixing ratio. In Fig. 7a, the set point at ~ 4.2 ppm H_2O , where the dispersion is the largest, occurs at $p_{\text{AIDA}} \sim 150$ hPa, while the set point at ~ 5.3 ppm H_2O occurs for $p_{\text{AIDA}} \sim 100$ hPa (see Fig. 3g). Spectroscopic techniques are sensitive to the environmental thermodynamic conditions, as the shape of the absorption line which is used to retrieve the mixing ratio depends on temperature and pressure. The measurement uncertainty is then also related to ambient conditions. In this case, the absorption depth is about 30 % larger at ~ 100 hPa compared to ~ 150 hPa. Hence, the instrument uncertainty is then better at lower pressures, and this leads to smaller variability in the retrievals.

$\text{H}_2\text{O} < 2$ ppm: in the lowest H_2O mixing ratio range, the limits of detection of the instruments can be assessed. Here, ALBATROSS and DLH achieve similar mean deviations (6 ± 8 % and 6 ± 9 %, respectively), with all set points of the blind intercomparison falling within a discrepancy of 20 % with respect to their references. For Pico-Light H_2O , the retrievals at $\text{H}_2\text{O} < 2$ ppm show a large and systematic moist bias with respect to the reference values, with a mean discrepancy exceeding +50 % (Table 3) and individual set points exceeding +100 %. The sensitivity of Pico-Light H_2O is further discussed in Appendix A5. SAWfPHY achieves a mean accuracy of -3 ± 2 %, although only two out of six set points were measured in this range due to the connection issues experienced by this instrument in BD3 (see Appendix A6).

Figure 8 shows a scatter plot of the reference H_2O mixing ratio and the mean chamber pressure level (p_{AIDA}) of each set point, color-coded with the absolute value of the mean relative difference ($|\Delta\text{H}_2\text{O}|$) of each instrument with respect to its reference and overlaid with two vertical profiles of H_2O mixing ratio in the atmosphere (as in Fig. 2). This highlights that for extractive instruments (ALBATROSS), the largest relative deviations occur at low H_2O mixing ratios and low pressures, where surface effects are enhanced, and hence an accurate determination of the H_2O mixing ratio is more difficult. Conversely, for in situ instruments (all others), the results are mainly affected by the H_2O mixing ratio range alone. Particularly, Pico-Light H_2O shows the largest discrepancies (> 20 %) at $\text{H}_2\text{O} < 2$ ppm and SAWfPHY at $\text{H}_2\text{O} > 100$ ppm (due to the dry bias in BD4), while DLH shows moderate discrepancies (< 20 % for all except one set point of the open intercomparison) throughout the entire investigated H_2O mixing ratio range.

Finally, it is worth noting that no significant differences are observed between the results of the open and blind intercomparison phases (see Figs. 6–8). This demonstrates that all instruments provide accurate measurements without the need of an independent measurement as a reference.

5.2 Precision

The precision of the instruments is evaluated by analyzing the time series of the set point measured at ~ 6 ppm H_2O and

~ 100 hPa pressure during OD3 (Fig. 7a, time ~ 6.4 h), representing average tropopause conditions. Figure 9 (left column) shows a zoom-in of the time series of H_2O mixing ratio at 2 s resolution measured during this period by all instruments (excluding SP-APicT, since the H_2O level considered here is well below the range of applicability of this instrument).

Following Fahey et al. (2014), a linear fit is applied to all time series (black dashed lines in Fig. 9, left column) to define the time evolution of the H_2O mixing ratio. This allows distinguishing instrumental variability from small changes in H_2O occurring inside the AIDA chamber and/or sampling lines during this interval. For the extractive instruments (MBW373LX and ALBATROSS), an additional sinusoidal fit is applied (solid black line in Fig. 9a, m) to account for the small-scale fluctuations in H_2O mixing ratio associated with the heating controller of the sampling line (discussed in the previous section). For SAWfPHY, due to a data gap that occurred during this set point, two individual linear fits are applied to describe the two intervals of the time series (see Fig. 9j). The exact form of the fitting equations and the corresponding parameters can be found in the Supplement (Sect. S3).

The resulting detrended time series (i.e., measured data – fit) are shown in Fig. 9 (middle column). The precision of each instrument is quantified by calculating the frequency of occurrence distributions (Fig. 9, right column) and standard deviation at 2 s resolution (σ_{2s}) of the detrended time series over the entire 10 min interval. The values of σ_{2s} obtained for each instrument are noted in the corresponding panels of Fig. 9 (right column) as both absolute and relative values (with respect to the mean of the considered instrument and set point). Note that the range of H_2O values shown in Fig. 9 is ± 0.1 ppm for all instruments except Pico-Light H_2O (Fig. 9g–i), for which a range of ± 1 ppm is shown. The frequency of occurrence distributions are calculated in bins of 5 ppb for all instruments and 50 ppb for Pico-Light H_2O (Fig. 9i).

Overall, Fig. 9 shows that a higher precision is achieved on average by the instruments based on frost-point hygrometry techniques (MBW373LX and SAWfPHY), with σ_{2s} of 6 and 7 ppb, respectively, corresponding to approximately 0.1 % of the measured H_2O mixing ratio. The laser spectrometers achieve precisions between 11 ppb (i.e., ~ 0.2 % of the measured signal) for APicT and ALBATROSS, 17 ppb (~ 0.3 %) for DLH, and 251 ppb (~ 4.7 %) for Pico-Light H_2O . All values obtained here are consistent with the uncertainty estimates given for each instrument in Table 1.

5.3 In-cloud measurements

In this section, we analyze the in-cloud measurements performed during BD2. As already mentioned, these measurements are particularly valuable since, assuming the ice cloud is dense enough to sustain $\text{RH}_{\text{ice}} = 100$ % in the chamber

Table 3. Summary of mean deviations and their standard deviation ($\mu \pm \sigma$) for each instrument during the blind intercomparison, calculated in five ranges of H₂O mixing ratio, along with the number of set points measured by each instrument in each range (N_{SP}). Note that the range of each set point is assigned for each participant instrument based on the mean H₂O mixing ratio of the reference instruments associated with that participant (i.e., Ref_{Ext} for ALBATROSS, Ref_{Int} for all other instruments).

H ₂ O range	ALBATROSS		DLH		Pico-Light		SAWfPHY	
	$\mu \pm \sigma$	N_{SP}	$\mu \pm \sigma$	N_{SP}	$\mu \pm \sigma$	N_{SP}	$\mu \pm \sigma$	N_{SP}
< 2 ppm	6 ± 8 %	5/5	6 ± 9 %	6/6	54 ± 55 %	5/6	−3 ± 2 %	2/6
2–10 ppm	8 ± 12 %	13/13	5 ± 5 %	13/13	−8 ± 5 %	13/13	−2 ± 3 %	6/13
10–100 ppm	0 ± 4 %	13/13	0 ± 2 %	12/12	−3 ± 9 %	11/12	−6 ± 12 %	11/12
> 100 ppm	−3 ± 1 %	9/9	0 ± 1 %	9/9	−4 ± 2 %	9/9	−7 ± 19 %	8/9
All set points	3 ± 9 %	40/40	3 ± 5 %	40/40	3 ± 28 %	38/40	−5 ± 13 %	27/40

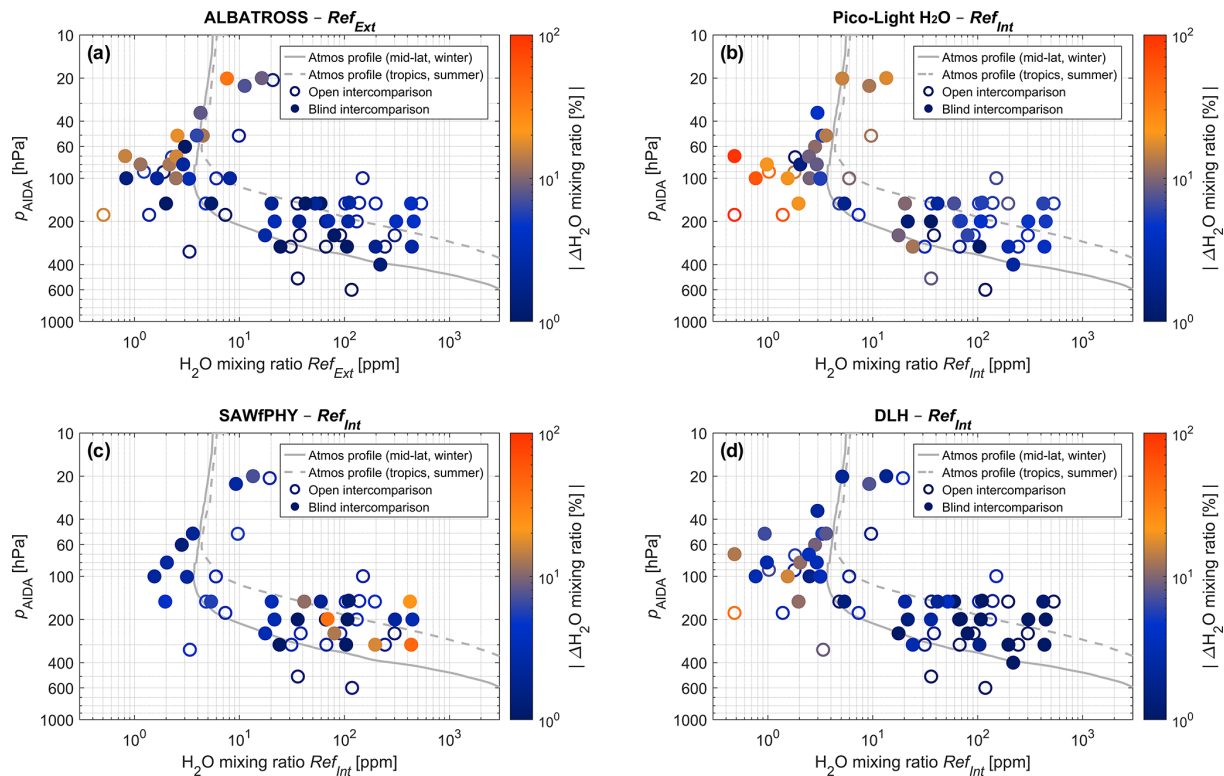


Figure 8. Scatter plot of p_{AIDA} against the reference H₂O mixing ratio (Ref_{Ext} for ALBATROSS, Ref_{Int} for all other instruments), color-coded with the absolute value of the mean relative difference ($|\mu|$) of each instrument with respect to its reference dataset, for all set points of the intercomparison, overlaid with two atmospheric profiles of H₂O mixing ratio (same as in Fig. 2). Open intercomparison set points are shown as empty dots, while blind intercomparison ones are shown as filled dots.

(e.g., Fahey et al., 2014), they provide an intrinsic reference for the gas-phase (in situ) instruments and hence allow validating the quality of the internal reference instruments.

To this end, the ice-saturated H₂O mixing ratio (H_2O_{IceSat}) was calculated based on the p_{AIDA} and T_{AIDA} measurements using Eq. (3), assuming $RH_{Ice} = 100\%$ and the parameterization for saturation vapor pressure over ice ($p_{Sat,Ice}$) from Murphy and Koop (2005). The uncertainty in H_2O_{IceSat} was also estimated based on the measurement uncertainties of p_{AIDA} and T_{AIDA} , which are 0.1 hPa in p_{AIDA} and 0.05 K

in T_{AIDA} , plus a contribution up to 0.3 K due to temperature inhomogeneity in the chamber (Möhler et al., 2003). Assuming that the two uncertainty contributions in T_{AIDA} are uncorrelated, this corresponds for the conditions analyzed here ($p_{AIDA} = 150$ hPa, $T_{AIDA} = 204$ K) to an uncertainty in H_2O_{IceSat} of $\pm 4.6\%$ (i.e., $H_2O_{IceSat} = 21.2 \pm 1.0$ ppm).

$$H_2O_{IceSat} = \frac{p_{Sat,Ice}(T_{AIDA})}{p_{AIDA}} \tag{3}$$

Figure 10a shows a time series of the H₂O mixing ratio measured by all instruments during BD2, along with H_2O_{IceSat}

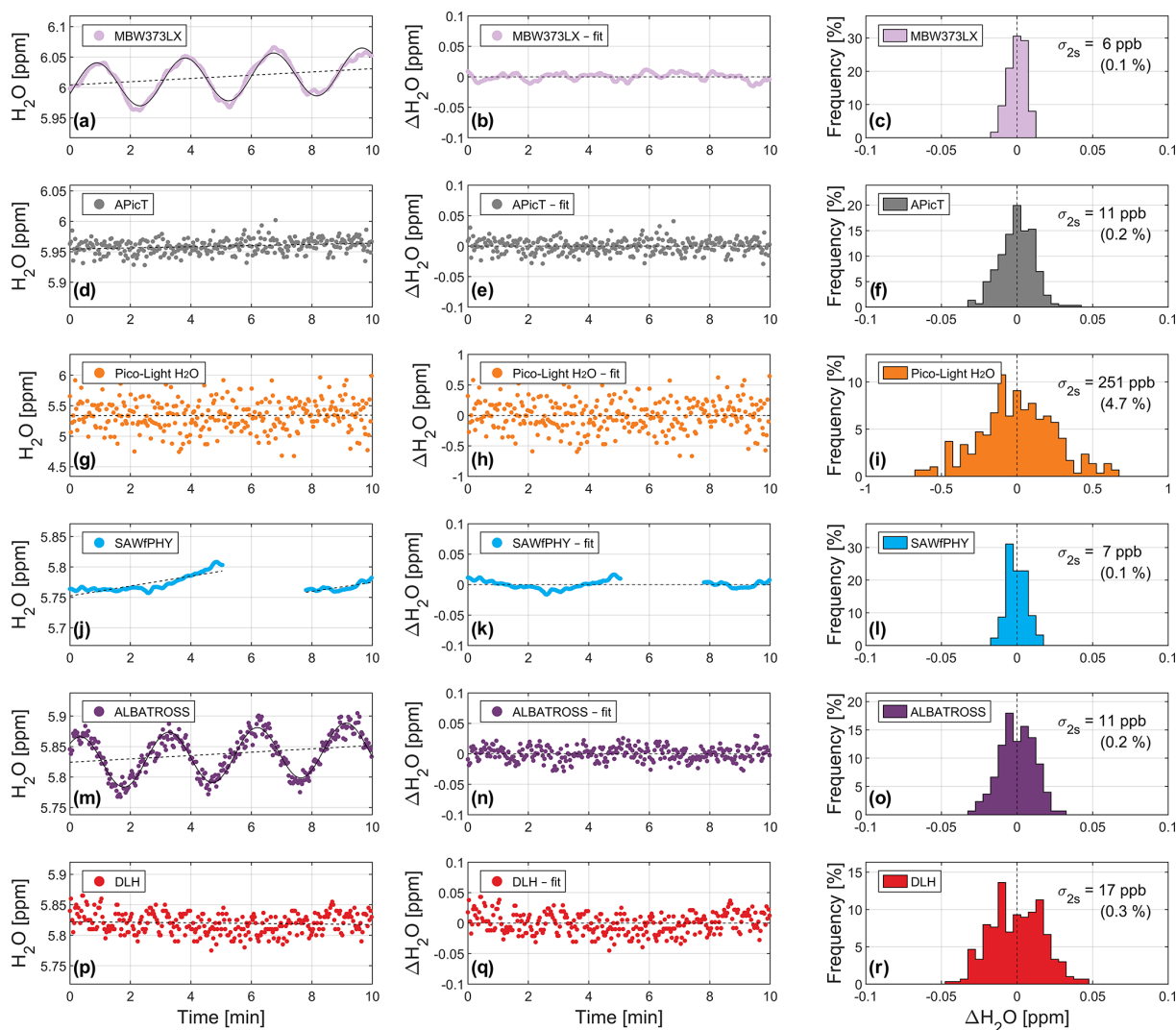


Figure 9. Precision analysis based on a set point measured at ~ 6 ppm H₂O and ~ 100 hPa pressure during OD3. Left column: time series of H₂O mixing ratio measured by all instruments (colored dots) and corresponding linear fits (black dashed lines). Sinusoidal fits performed additionally for MBW373LX and ALBATROSS are shown as solid black lines (a, m). Middle column: detrended time series (i.e., difference between measured signals and the fitted curves). Right column: frequency of occurrence distributions, calculated in bins of 5 ppb (all instruments) and 50 ppb (Pico-Light H₂O, i). The standard deviation at 2 s resolution (σ_{2s}) is noted for each instrument in the corresponding panel (as both absolute and relative values).

calculated from p_{AIDA} and T_{AIDA} (black line) and its uncertainty (green shading), while Fig. 9b shows a zoom into the interval of ice cloud occurrence. The cloud is generated upon addition of H₂O into the chamber at constant p_{AIDA} and T_{AIDA} at time ~ 6.5 h. After the cloud formation, the gas-phase H₂O mixing ratio measured by all in situ instruments is in good agreement with the ice-saturated mixing ratio at around 21 ppm H₂O, while the total H₂O content measured by the extractive instruments increases up to around 50 ppm, indicating an ice water content of approximately 30 ppm H₂O. Then, the total H₂O decreases with time as the cloud sublimates due to warming from the chamber walls (sedimentation may also contribute, depending on ice parti-

cle size), while gas-phase H₂O remains stable until about the time of 7.1 h (see Fig. 10b). This indicates that the ice cloud was stable and dense enough to sustain $RH_{ice} = 100\%$ in the chamber for approximately 40 min.

Figure 10c–d show the relative differences in gas-phase H₂O between all internal instruments and H₂O_{IceSat} (panel c) and the relative difference in total H₂O between ALBATROSS and MBW373LX (d) for the same time interval. All the in situ instrument measurements during the cloud occurrence interval fall within $\pm 5\%$ with respect to H₂O_{IceSat}. Particularly, APicT overestimates the ice-saturated H₂O mixing ratio by +5 %, which is at the upper edge of its nominal uncertainty range specified in Table 1. Pico-Light H₂O un-

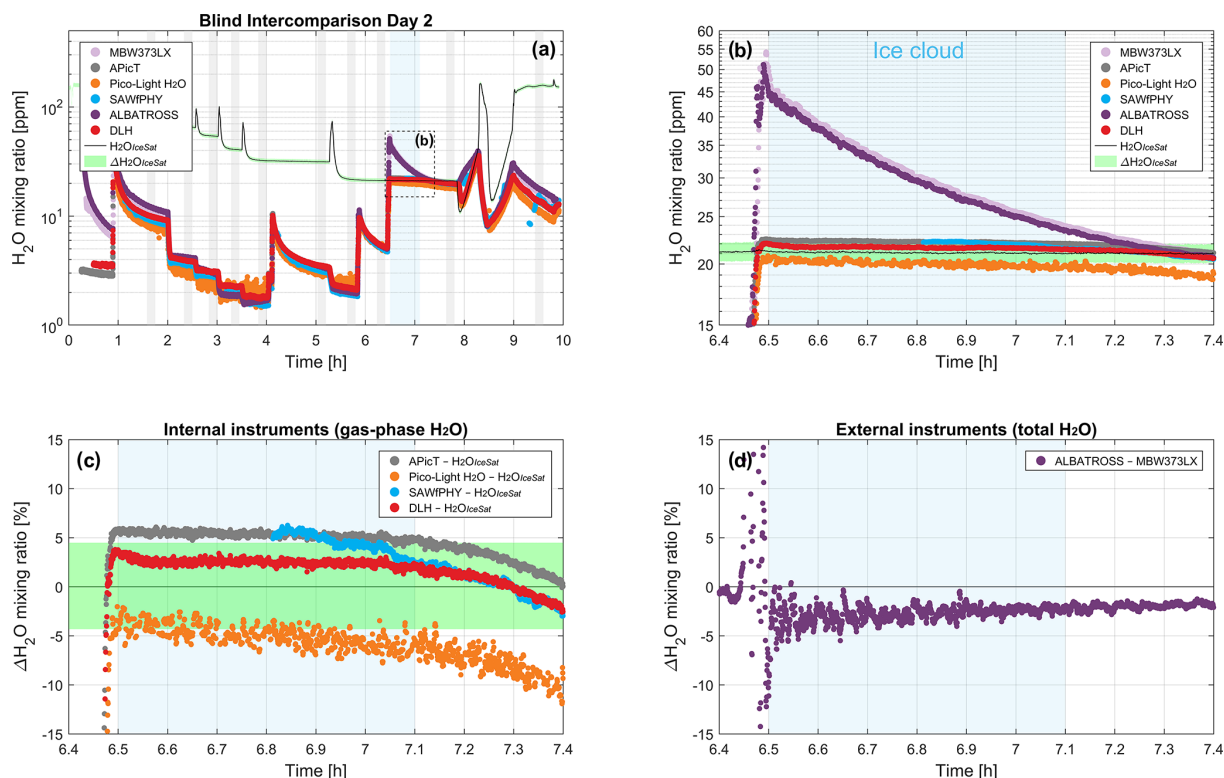


Figure 10. In-cloud measurement analysis. **(a)** Time series of H₂O mixing ratio measured by all instruments during BD2 (same as Fig. 4b), along with the ice-saturated H₂O mixing ratio ($H_{2O_{IceSat}}$) calculated from p_{AIDA} and T_{AIDA} (black line) and its uncertainty (green shading). **(b)** Zoom into the ice cloud occurrence interval. **(c)** Relative differences (in percent) in gas-phase H₂O between all in situ instruments (APicT, SP-APicT, Pico-Light H₂O, SAWfPHY, DLH) and $H_{2O_{IceSat}}$. **(d)** Relative difference in total H₂O between the external instruments ALBATROSS and MBW373LX. In all panels, the blue shaded area highlights the interval of ice cloud occurrence (relative time 6.5–7.1 h).

derestimates $H_{2O_{IceSat}}$ by -5% , while DLH shows an average deviation of approximately $+2.5\%$ (i.e., within the $\pm 4.6\%$ uncertainty in $H_{2O_{IceSat}}$ based on p_{AIDA} and T_{AIDA}), and SAWfPHY varies between $+5\%$ and $+2.5\%$ (with a measurement gap in the first ~ 20 min after cloud formation). The relative difference in total H₂O between ALBATROSS and MBW373LX ranges between -4% and -2% (Fig. 10d).

6 Conclusions

The AquaVIT-4 campaign continues the valuable efforts of the AquaVIT intercomparison series to assess the performance of atmospheric hygrometers for water vapor measurements in the upper atmosphere. This intercomparison involved four airborne hygrometers, deployed on aircraft or stratospheric balloon platforms and using either laser absorption spectroscopy or frost-point hygrometry techniques, which were compared with three in-house reference instruments at the AIDA chamber. This campaign provided an excellent opportunity to test new techniques, such as the Surface-Acoustic Wave frost-Point hygrometer (SAWfPHY) and the QCL-based ALBATROSS spectrometer, alongside

established instruments, like the Pico-Light H₂O (successor of the former Pico-SDLA) and the DLH spectrometer.

A strong focus was placed on simulating realistic UTLS conditions in the AIDA chamber (pressure 20–600 hPa, temperature 190–245 K, H₂O mixing ratio 0.5–530 ppm) and defining reference values for each static interval. Repeated measurements of the various experimental conditions highlight the need to distinguish between in situ and extractive methods due to adsorption/desorption effects of H₂O in the sampling line of the extractive instruments and as such to define separate references for them. Specifically, in situ instruments (DLH, Pico-Light H₂O, SAWfPHY) are compared with the APicT and SP-APicT reference spectrometers for set points in the range of $H_2O < 100$ ppm and $H_2O > 100$ ppm, respectively, whereas extractive instruments (ALBATROSS) are compared with the MBW373LX dew-point mirror hygrometer.

The statistical analysis shows that for $H_2O > 100$ ppm, most instruments (ALBATROSS, Pico-Light H₂O, DLH) achieve mean deviation smaller than $\pm 4\%$ from the reference, while SAWfPHY shows larger discrepancies (between 10%–20%) for three individual set points. In the 10–100 ppm H₂O range, all instruments are in good agreement,

with mean deviations within $\pm 7\%$ from the reference. This performance is also maintained in the range of 2–10 ppm H_2O , with mean deviations within $\pm 8\%$, while the relative standard deviations tend to increase due to the reduced H_2O content. The largest differences were found in the range of $\text{H}_2\text{O} < 2$ ppm, particularly for Pico-Light H_2O , which was not designed for such low mixing ratios. DLH, ALBATROSS, and SAWfPHY also achieve a good performance (within $\pm 10\%$) below 2 ppm H_2O .

For context, the subset of “core” instruments in AquaVIT-1 was found to agree to within $\pm 10\%$ with the reference in the range 1–150 ppm H_2O and showed differences of -100% to $+150\%$ in the range $\text{H}_2\text{O} < 1$ ppm (Fahey et al., 2014). While a direct comparison with these results is difficult due to the different reference value definitions, in general we observe slightly smaller mean deviations for the instruments participating in AquaVIT-4, in the range of both $\text{H}_2\text{O} > 10$ ppm ($\pm 7\%$) and 2–10 ppm H_2O ($\pm 7\%$), with respect to the AquaVIT-1 “core” instruments ($\pm 10\%$). It is also remarkable that, unlike most of the AquaVIT-1 “core” instruments, the AquaVIT-4 instruments (DLH, ALBATROSS, SAWfPHY) achieve good agreement ($\pm 10\%$) at $\text{H}_2\text{O} < 2$ ppm as well.

The measurement precision at 2 s resolution (σ_{2s}) was evaluated for all instruments at average tropopause conditions (~ 6 ppm H_2O and 100 hPa pressure). This shows that a higher precision (6–7 ppb, corresponding to approximately 0.1 % of the measured H_2O mixing ratio) is achieved on average by the instruments based on frost-point hygrometry techniques (MBW373LX and SAWfPHY). The laser spectrometers achieve precisions of 11 ppb (i.e., $\sim 0.2\%$: APiCT and ALBATROSS), 17 ppb ($\sim 0.3\%$: DLH), and ~ 250 ppb ($\sim 4.7\%$: Pico-Light H_2O).

Of special interest were in-cloud conditions, i.e., intervals where ice saturation was reached and an ice cloud has been produced in the AIDA chamber. A detailed analysis of one of these intervals, where a dense ice cloud persisted for about 40 min, showed that all in situ (gas-phase) instruments fell within $\pm 5\%$ of the calculated ice saturation mixing ratio, which stands at the outer bound of the saturation mixing ratio uncertainty ($\sim 4.6\%$, dominated by the uncertainty in measured air temperature). This demonstrates the reliability of the hygrometers in probing ice-saturated conditions. Correspondingly, these instruments, if equipped with a highly accurate temperature sensor, can be used to study dehydrating processes across the tropopause. The $\pm 5\%$ agreement of APiCT with respect to the calculated ice saturation H_2O mixing ratio is consistent with the ice-saturated experiments performed in AquaVIT-1 (see Fig. A2 in Fahey et al., 2014), demonstrating that the performance of this instrument is preserved from the past AquaVIT-1 intercomparison.

In general, the observed agreement with the reference instruments was satisfactory for all the participants.

- For ALBATROSS, the deviations from MBW373LX obtained here fall within the expected range, although they are larger compared to a previous laboratory-based validation against SI-traceable reference gases (Brunamonti et al., 2023). This can be attributed to the uncertainty related to the residual water content (typically < 1 ppm) in the cell, originating from surface desorption effects along the sampling line. While these effects can be compensated for by measuring a dry-air spectrum (Brunamonti et al., 2023), during AquaVIT-4 it was not possible to verify the zero level between the dynamic pressure conditions of the AIDA chamber due to the very long equilibration times. Therefore, the “background” H_2O contribution was determined overnight and parameterized as a function of cell pressure. This procedure, detailed in Appendix A3, can result in an uncertainty of up to ± 0.2 ppm in the retrieved mixing ratios (i.e., $\pm 20\%$ at 1 ppm H_2O), especially at low pressures ($p_{\text{AIDA}} \sim 20$ hPa), which is about 10-fold larger than the analytical precision of ALBATROSS at these concentrations. It is important to note that these effects do not apply during flight conditions, where ALBATROSS operates in an open-path configuration (e.g., Graf et al., 2021), i.e., without any sampling line and with a gas flow 3 orders of magnitude larger. Hence, the surface in contact with the gas is substantially smaller, and artifacts due to surface adsorption/desorption effects are negligible.
- The performance of DLH is in line with expectations based on prior in-flight performance. As described in Sect. 3.2, the installation of DLH in the AIDA facility required the introduction of an additional window in the optical beam path and with it the possibility of optical interference not present in the flight configuration, as well as an additional path between the instrument and the facility window which had to be kept sufficiently dry so as not to introduce an offset in the measured concentration. The size of the chamber limited the measurement absorption path length to approximately 9.41 m, reducing the measurement sensitivity to between 52 % and 72 % of what it would be on the WB-57 aircraft. Despite these adaptations necessary to operate in the AIDA facility, DLH instrument performance appears to have met its stated accuracy and precision metrics during the AquaVIT-4 campaign.
- The Pico-Light H_2O hygrometer is the successor of the former Pico-SDLA, which was operated during AquaVIT-1. In the range of $\text{H}_2\text{O} > 100$ ppm, the Pico-SDLA agreed with the reference to within $\pm 10\%$ on average (Fahey et al., 2014), while in AquaVIT-4, the agreement of Pico-Light H_2O falls within $\pm 4\%$. In the range of 2–10 ppm H_2O , during AquaVIT-1, Pico-SDLA had a tendency to overestimate mixing ratios, ranging from 20 % to more than 100 %. During

AquaVIT-4, the agreement falls in the $\pm 8\%$ range. The largest discrepancies observed during AquaVIT-1 were due to the simulated mixing ratios being drier than normal at the given pressure levels. In such cases, the absorption line depicts a flat broad shape which renders it difficult to separate the absorption signal from the spectrum baseline (zero absorption zones) and leads to large errors. During AquaVIT-4, the overestimations are reduced due to the fact that low mixing ratios have been simulated mainly at low p_{AIDA} (10–150 hPa), where the line width permits a better identification of the zero absorption zones. For $\text{H}_2\text{O} < 2$ ppm, due to the short path length (1 m), the sensitivity of the hygrometer is not sufficient. The limit of quantification (10σ) of the instrument is estimated to be about 0.8 ppm H_2O , close to the simulated conditions (see Appendix A5). The results of AquaVIT-4 are mostly in line with previous balloon-borne comparisons, i.e., within the $\pm 10\%$ range at UTLS conditions, though slightly larger than the claimed total uncertainty (see Ghysels et al., 2024: total uncertainty scaling from 4.4 % to 12 % between 200 and 10 hPa).

- SAWfPHY has been specifically designed to perform water vapor measurements on board long-duration balloons flying in the tropical lower stratosphere. The instrument is therefore optimized for measurements in the sub-10 ppm H_2O mixing ratios. In this range, SAWfPHY's measurements during both the open and blind periods of the AquaVIT-4 campaign achieved excellent accuracy and precision ($< 3\%$ down to 1.5 ppm) and are in line with the expected instrument performances. The specific configuration of SAWfPHY used in the AIDA chamber prevented the instrument from making measurements during some set points falling in this mixing ratio range. These limitations, however, do not apply to balloon flights (see Appendix A6), where observations have been recorded at temperatures comparable to the lowest ones experienced during the AquaVIT-4 campaign. SAWfPHY performances at mixing ratios higher than 10 ppm are generally in line with those in the sub-10 ppm range, except for a few set points that contribute to degrading the overall statistics. These lower-accuracy measurements directly result from the choices made in the instrument design and operations in the tropical lower stratosphere (see Appendix A6 for further details).

Overall, the AquaVIT-4 campaign demonstrated the high accuracy and reliability of the four involved sensors for atmospheric monitoring and research applications at a wide range of UTLS-relevant conditions. Here, it is also important to compare the results with the requirements for upper-air H_2O measurement uncertainty defined by the GCOS Implementation Plan 2022 (GCOS, 2022). Based on the mean deviations found in this work (not considering vertical resolu-

tion), all instruments achieve at least the “threshold” level defined by GCOS (i.e., $\pm 10\%$) at all conditions (except for Pico-Light H_2O below 2 ppm), which qualifies the data as useful in terms of climate monitoring studies. Regarding the “breakthrough” and “goal” levels, we observe that the criteria that define these levels (2 %–5 %) are of the same magnitude as the uncertainty of the reference instruments used here (see Table 1), which are state-of-the-art hygrometers in a well-controlled laboratory setting such as the AIDA chamber. Hence, although mean deviations smaller than 2 %–5 % are achieved by the instruments in individual H_2O ranges, an absolute assessment of these criteria is limited by the available reference methods.

Appendix A: Data post-processing, calibration, and instrument-specific issues

A1 APicT, SP-APicT

The measurements with APicT and SP-APicT were done with 140 Hz and averaged to 1 s time resolution. The water absorption line profile of the 000-101 to 110-211 transition at 7299.43 cm^{-1} was fitted online with a Voigt profile based on line parameters from the HITRAN database (Rothman et al., 2013) and the actual temperature and pressure measured in the AIDA chamber. No calibration was conducted and the absolute accuracy estimated from an error budget is better than 5 % and dominated by the line strength uncertainty ($\pm 3\%$) (Fahey et al., 2014). Please note that the data used here were not post-processed and the “additional” water absorption in the laser was not subtracted. Therefore, the values at lowest water concentrations can show a high bias, which is especially visible for SP-APicT data for mixing ratios below 20 ppm.

A2 MBW373LX

The data from the chilled-mirror hygrometer (MBW373LX, MBW calibration AG) were recorded online with a nominal time resolution of 1 s and an accuracy given by the manufacturer of ± 0.1 K frost point, which corresponds to an accuracy in water partial pressure ranging from $\pm 0.8\%$ at 273 K to $\pm 1.8\%$ at 183 K (Murphy and Koop, 2005). The instrument was calibrated by the manufacturer on July 2020 in the range of 193 to 274 K (certificate: 8043MBW2020), documenting the traceability to national standards.

A3 ALBATROSS

During AquaVIT-4, ALBATROSS was operated in a closed-path configuration, as described in Brunamonti et al. (2023). Such an extractive configuration is only used for laboratory measurements, whereas for in-flight applications, the instrument is operated in an open-path configuration (Graf et al., 2021). In open-path configuration, the measurement

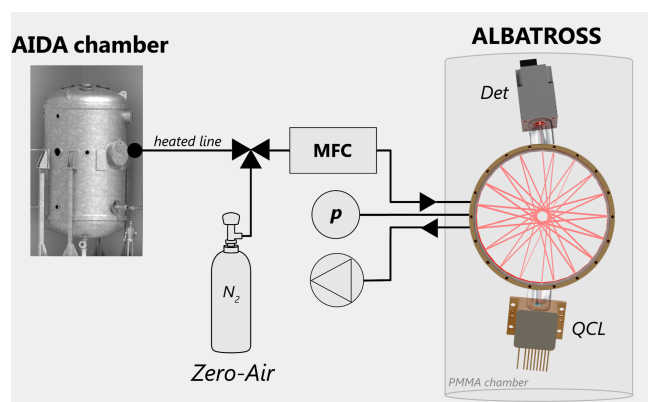


Figure A1. Schematics of the sampling system used for ALBATROSS in AquaVIT-4.

takes place in situ at flow rates 3 orders of magnitude larger (~ 1500 vs 0.5 SLM), and the surface in contact with the gas is negligible. Therefore, the artifacts due to the adsorption/desorption of H_2O molecules do not apply. The main reason for the extractive approach is due to the delicate electronics (DAQ, FPGA) and sensitive optical elements (IR detector and QCL, requiring a temperature stability at mK level). While balloon flights typically last less than 3 h, a period at which the implemented onboard heat management can be fully maintained, continuous operation under low temperatures over 2 weeks, as in the case of the AIDA chamber, is not supported.

A schematic of the sampling system used for ALBATROSS in AquaVIT-4 is shown in Fig. A1. The segmented circular multipass cell (SC-MPC) is closed on both sides by electropolished stainless-steel lids, treated by a highly inert coating (SilcoNert[®] 2000, SilcoTek, USA) to minimize the adsorption of H_2O molecules on their surface. The sample gas is extracted from the AIDA chamber by a vacuum pump through a heated sampling line. The instrument is operated inside a custom-made PMMA plastic chamber to suppress any sudden temperature or humidity fluctuations. The pressure in the multipass cell (p_{Cell}) is monitored by a heated capacitance manometer (AA02, MKS Instruments, USA), with an absolute accuracy of 0.12% . The flow rate extracted from the AIDA chamber, and therefore p_{Cell} , varied during each experiment depending on the AIDA pressure. A mass-flow controller (MFC) upstream of the SC-MPC was used to constrain the flow rate to a maximum of 0.5 SLM (corresponding to $p_{\text{AIDA}} \sim 300$ hPa). Hence, all measurements at $p_{\text{AIDA}} > 300$ hPa were performed at a constant flow rate (0.5 SLM) and p_{Cell} (~ 45 hPa), while for $p_{\text{AIDA}} < 300$ hPa, the flow rate and p_{Cell} varied between 0.02 – 0.5 SLM and 10 – 45 hPa, respectively (with p_{AIDA} in the range of 20 – 300 hPa).

For the spectroscopic retrieval, the raw spectra are normalized to account for the laser intensity variation across the scanning range (baseline) and, in closed-path configura-

tion, the “zero-air” H_2O contribution, i.e., the residual water content (typically < 1 ppm) in the cell due to surface desorption effects along the sampling line. The normalization can be done either by reconstructing the laser intensity baseline using a polynomial function (Graf et al., 2021) or by dividing each raw spectrum by the corresponding zero-air spectrum (i.e., the transmission through the multipass cell filled with N_2 6.0) (Brunamonti et al., 2023). The second approach has the advantage that it simultaneously accounts for both the intensity baseline and the zero-air contributions. As this second contribution is pressure-dependent, it requires individual zero-air spectrum measurements for each investigated pressure level. During AquaVIT-4, due to the dynamic pressure conditions of the AIDA chamber, direct access to such a “zero-air” spectrum for each established pressure level was not possible due to the long equilibration times. Therefore, we adopted the polynomial baseline approach and subtracted the zero-air H_2O contribution after the spectroscopic retrieval based on dry N_2 (purity 6.0) measurements performed overnight between the experiments.

Figure A2 shows an overview of the nighttime measurement routine between BD2 and BD3. The zero-air spectra are acquired by measuring N_2 at varying flow rate and pressure conditions. The resulting correction is then parameterized as a function of p_{Cell} and subtracted from the retrieved H_2O amount fractions. The MFC was programmed to scan the range 0 – 0.5 SLM in 32 steps of 10 min each, corresponding to 5 – 45 hPa in p_{Cell} , which covers the entire range of variability of p_{AIDA} during the daytime experiments. As expected, the zero-air H_2O mixing ratio (panel d) shows an exponential dependency on p_{Cell} , varying from about 10 ppm at $p_{\text{Cell}} \sim 5$ hPa (corresponding to $p_{\text{AIDA}} \sim 15$ hPa) to 0.7 ppm at $p_{\text{Cell}} \sim 45$ hPa ($p_{\text{AIDA}} \geq 300$ hPa). The correction is calculated by fitting this behavior using an exponential function. Zero-air measurements were repeated every night during the campaign, showing a slight tendency towards lower H_2O amount fractions with time.

The spectral fitting was performed using a quadratic speed-dependent Voigt profile (qSDVP) line shape model, with the optimized pressure broadening parameters (Γ_0 and Γ_2) derived by Brunamonti et al. (2023) and line strength parameter from the HITRAN2020 database (Gordon et al., 2022). This approach was found to substantially improve the accuracy of the instrument compared to the standard Voigt profile, in particular by removing pressure-related artifacts (Brunamonti et al., 2023).

The zero-level correction described here represents the major source of uncertainty of the AquaVIT-4 measurements. Figure 11e shows that this uncertainty is smaller than ± 0.1 ppm at most conditions but increases to ± 0.2 ppm (i.e., $\pm 20\%$ at 1 ppm H_2O) at low pressures ($p_{\text{AIDA}} \sim 20$ hPa). Again, it should be noted that this procedure is not needed in normal open-path flight configuration.

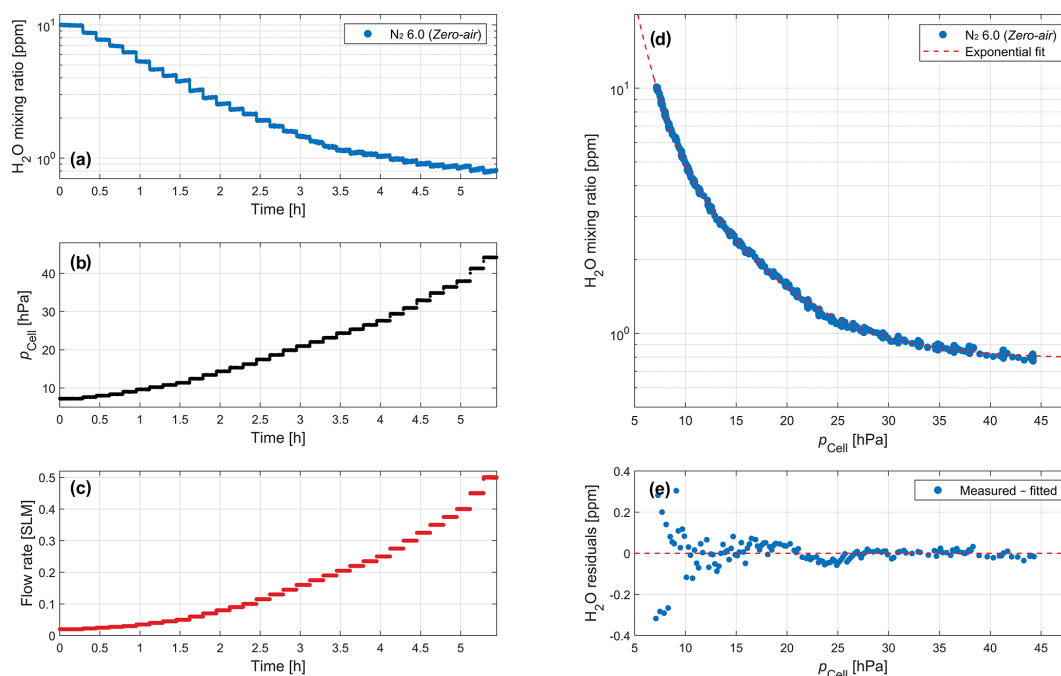


Figure A2. Overview of the nighttime ALBATROSS zero-air (N_2 6.0) measurements performed between BD2 and BD3. **(a–c)** Time series of the measured H_2O mixing ratio, cell pressure (p_{Cell}), and flow rate, respectively. **(d)** H_2O mixing ratio in the zero air as a function of p_{Cell} (blue markers) and exponential fit (red line), as well as the associated fit residuals **(e)**.

A4 DLH

For each aircraft or ground facility and each campaign, the DLH second harmonic absorption signal is converted to water vapor mixing ratio using quality-controlled temperature and pressure data and the measured optical path length. Using a WMS instrument model developed at NASA Langley, the range of temperatures and pressures for a given campaign, and a range of water vapor mixing ratios appropriate to each temperature and pressure, a matrix of line-center WMS 2f signal vs. (p , T , H_2O) is generated. Such a matrix is created for each absorption line and for each set of WMS parameters. From these matrices, a multidimensional curve fit is created of the form $\text{H}_2\text{O} = f(p, T, \text{signal, line, operational parameters})$. Each data point during the AquaVIT-4 time period was converted in this way. All data were reported, except for time periods when the laser was not actively measuring water vapor. During the non-blind operating time period, opportunities were taken to collect data meant to improve DLH signal conversion, and data recorded during those time periods were not archived. Despite this, DLH data were reported during all blind and non-blind comparison periods.

A5 Pico-Light H_2O

The Pico-Light H_2O hygrometer was located 1 m away for the SAWPHY hygrometer in the main vessel. The optical cell was located in the main chamber and the electronic box was located in the laboratory space. The electronic

box has been optimized to accommodate short-duration (2–3 h) flights under radiosounding balloons, rather than long-duration balloon flights (as in Strateole-2). In the configuration of radiosounding flights, the electronics box needs less thermal insulation, and its heat capacity is sufficient to keep its temperature above the minimum operating temperature during the entire flight. Using less thermal insulation contributes to the decrease in weight. In the case of AquaVIT-4, the instrument remains at low temperatures for several days. In such a configuration, the electronic box was transported to the laboratory space to prevent damage to the electronics of the instrument. To reproduce real flight configurations of the instrument, an empty electronic box replaced the real one in the main vessel in order to address potential contamination effects.

The instrument acquires one unitary spectrum every 30 ms. The dataset provided for the open and blind intercomparison are the retrievals from the unitary spectra using Pico-Light H_2O internal pressure and temperature measurements. The H_2O measurements are taken at 1 s intervals. During that interval, 200 ms are devoted to recording the elementary atmospheric spectrum (within this time frame, five spectra are recorded), which comprises 1024 data points. The remaining 800 ms are used to record the atmospheric pressure and temperature, the GPS data, and the status of the instrument.

The mixing ratio is extracted from the absorption spectrum using a nonlinear least-squares fitting algorithm applied to the full line shape based on the Beer–Lambert law and in con-

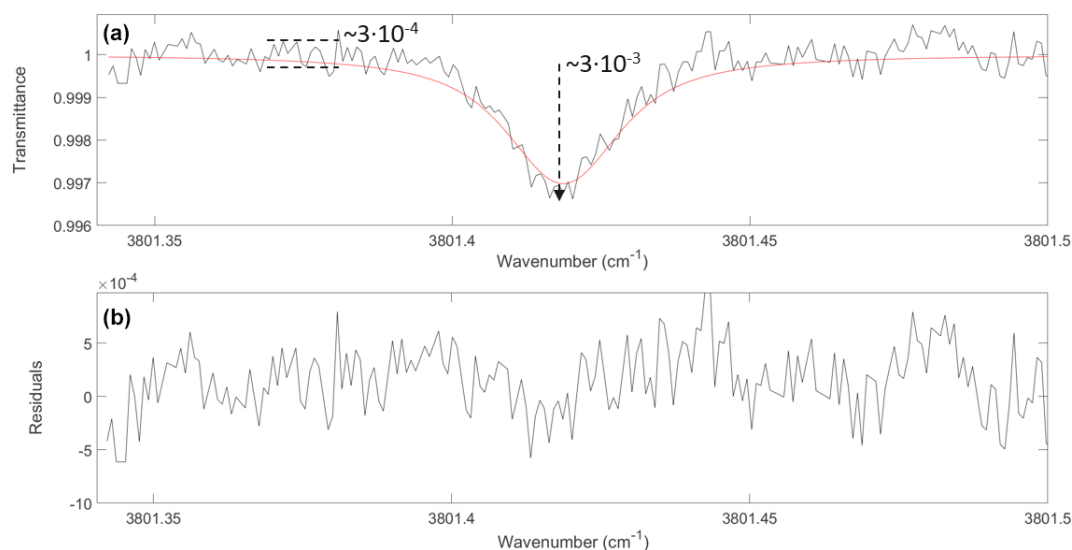


Figure A3. Pico-Light H₂O unitary spectrum (10 ms integration time) of the “stratospheric line” at 3801.41863 cm^{−1} during BD3 at extremely dry conditions ($p_{\text{AIDA}} = 71.5$ hPa, $T_{\text{AIDA}} = 190.5$ K, 0.81 ppm H₂O) (a) and corresponding fit residuals (b).

junction with in situ pressure and temperature measurements (Voigt profile). During a flight, two spectroscopic transitions are needed to probe both the troposphere and stratosphere: the $2_{02} \leftarrow 1_{01}$ (3801.41863 cm^{−1}, “stratospheric line”) and the $4_{13} \leftarrow 4_{14}$ (3802.96561 cm^{−1}, “tropospheric line”) lines. During AquaVIT-4, set points simulated atmospheric conditions in the upper air. Therefore, only the stratospheric line was used. The line strength of the stratospheric line is about 10 times larger than the one of the tropospheric line.

The Pico-Light H₂O dataset of part of BD4 (after relative time ~ 3 h) was revised after the disclosure of the results. This is because the automatic data processing routine used to retrieve the mixing ratios from the recorded spectra was set to choose the tropospheric line instead of the stratospheric line based on the measured air pressure (which is the approach used for flight data). However, as already mentioned, only the stratospheric line was used for AquaVIT-4. As a consequence, the retrieved mixing ratios were 10 times larger than expected. Therefore, the data were then reprocessed using the appropriate spectral line, and the revised retrievals were shared with the other participants and referees and used in this paper.

Figure A3 shows an example of a unitary spectrum recorded during BD3 for $p_{\text{AIDA}} = 71.5$ hPa, $T_{\text{AIDA}} = 190.5$ K, and H₂O mixing ratio = 0.81 ppm. This shows that the driest conditions simulated during AquaVIT-4 are close to the quantification limit of the instrument. The absorption depth of the stratospheric line is roughly 10 times larger than the noise level of the spectra. In such conditions, the instrument uncertainty increases. The precision of the mixing ratio is about 0.28 ppm (no averaging), about 3 times smaller than the simulated mixing ratio. The total uncertainty for a mixing ratio smaller than 1 ppm reaches 15 %–20 %.

A6 SAWfPHY

Despite the excellent accuracy for most of the water vapor measurements performed by SAWfPHY, the instrument experienced a number of issues and did not report measurements for some of the set points during both the AquaVIT-4 campaign weeks. We provide more details on these events.

First, as already mentioned, the instrument experienced electrical issues between the electronics outside the vessel and the sensing chamber inside AIDA. These issues prevented any SAWfPHY measurements during the 2 coldest days (OD4 and BD3), leading to 12 missed set points in the range 0.5–3 ppm H₂O. Yet, SAWfPHY reported measurements for H₂O mixing ratios as low as 1.5 ppm during BD2, which are already rarely observed in the lower stratosphere. Another four set points at H₂O mixing ratios < 5 ppm were missed by SAWfPHY at the beginning of BD1. These set points were associated with a difference between the AIDA and the frost-point temperatures larger than 30 K. Since SAWfPHY is a low-power instrument, the Peltier device that cools the sensing surface is hardly able to provide such temperature difference. This did not prevent SAWfPHY from making measurements in the lower stratosphere during long-duration balloon flights as the difference between the frost point and the air temperature is generally lower than 25 K there. In addition, part of this difference during balloon flights is achieved in a passive way by the radiator connected to the warm face of the Peltier element, which radiatively cools to space.

The SAWfPHY lowest-precision measurements took place at H₂O mixing ratios > 40 ppm. Those departures from the reference instrument are associated with SAWfPHY’s control loop of the sensing device temperature, which has been

optimized for lower-stratospheric mixing ratios. The control loop of frost-point hygrometers is designed to compensate for the mass evolution of the condensate by adjusting the temperature of the sensing device. The temperature variations imposed by the control loop translate into a mass flux out of or into the condensate. For a given temperature variation, the more water available in the gas phase, the larger the mass flux. Hence, in order to measure H₂O mixing ratios of a few ppm in a reasonable time, SAWfPHY's control loop has to be quite responsive, which can be detrimental at higher mixing ratios and lead to lower precision.

Last, a distinct issue occurred in BD4, during which the AIDA temperature set point was higher than -40°C . We discovered once the blind results were revealed that SAWfPHY mixing ratios started to be strongly underestimated after a large injection of water in the AIDA vessel (about 5 h after the start of the experiment on that day). During this injection, the instrument control loop actually warmed the sensing surface of the instrument in order to maintain a constant mass of deposit on the sensing device. The sensing surface eventually reached temperatures higher than -40°C so that the ice deposit fully sublimated (or melted). A hypothesis for the subsequent underestimated measurements is that supercooled water droplets might have grown as a new condensate. Consequently, from that time on, we corrected SAWfPHY's measurements by using the saturation vapor pressure over supercooled water (Murphy and Koop, 2005) rather than over ice as is generally applied. This significantly improved the comparison with the reference instrument, yet not perfectly. In any case, this issue is common to frost-point hygrometers, which generally have no way of knowing the phase of the condensate and work best at temperatures lower than -40°C or need to develop specific measurement strategies above -40°C (e.g., Vömel et al., 2016).

Data availability. The data are available via the KIT open data repository (<https://doi.org/10.35097/e7yxjpyc8xyv1ga4>, Brunamonti et al., 2025).

Supplement. The supplement related to this article is available online at <https://doi.org/10.5194/amt-18-5321-2025-supplement>.

Author contributions. MG coordinated the AquaVIT-4 project and led the organization of the intercomparison campaign. SB merged the final datasets, performed the data analysis, and generated all figures. HS controlled the AIDA chamber operation, supported the installation of all instruments, and performed the reference measurements. MG, NA, RB, and FF operated the Pico-Light H₂O instrument and analyzed the data. SB, BT, and LE operated the ALBA-TROSS instrument and analyzed the data. AH, PM, CC, and JL operated the SAWfPHY instrument and analyzed the data. GD operated the DLH instrument and analyzed the data. MF, OM, and KR

acted as independent referees for the blind intercomparison. SB and MG wrote the paper with contributions from all authors.

Competing interests. The contact author has declared that none of the authors has any competing interests.

Disclaimer. Publisher's note: Copernicus Publications remains neutral with regard to jurisdictional claims made in the text, published maps, institutional affiliations, or any other geographical representation in this paper. While Copernicus Publications makes every effort to include appropriate place names, the final responsibility lies with the authors. Views expressed in the text are those of the authors and do not necessarily reflect the views of the publisher.

Acknowledgements. The authors gratefully acknowledge technical support by the AIDA team at KIT. The authors thank Julian Gisler (Empa) for his support in creating the graphics of Figs. 1 and A1.

Financial support. This work was supported by the European Commission under the Horizon 2020 – Research and Innovation Framework Programme, through the ATMO-ACCESS Integrating Activity under grant agreement no. 101008004. The ALBA-TROSS participation was further supported within the framework of GAW/GCOS-CH (Swiss H₂O-Hub project). The article processing charges for this open-access publication were covered by Empa (Switzerland).

Review statement. This paper was edited by Dwayne Heard and reviewed by two anonymous referees.

References

- Banerjee, A., Chiodo, G., Previdi, M., Ponater, M., Conley, A. J., and Polvani, L. M.: Stratospheric water vapor: an important climate feedback, *Clim. Dynam.*, 53, 1697–1710, <https://doi.org/10.1007/s00382-019-04721-4>, 2019.
- Brunamonti, S., Jorge, T., Oelsner, P., Hanumanthu, S., Singh, B. B., Kumar, K. R., Sonbawne, S., Meier, S., Singh, D., Wienhold, F. G., Luo, B. P., Boettcher, M., Poltera, Y., Jauhainen, H., Kayastha, R., Karmacharya, J., Dirksen, R., Naja, M., Rex, M., Fadnavis, S., and Peter, T.: Balloon-borne measurements of temperature, water vapor, ozone and aerosol backscatter on the southern slopes of the Himalayas during StratoClim 2016–2017, *Atmos. Chem. Phys.*, 18, 15937–15957, <https://doi.org/10.5194/acp-18-15937-2018>, 2018.
- Brunamonti, S., Füzér, L., Jorge, T., Poltera, Y., Oelsner, P., Meier, S., Dirksen, R., Naja, M., Fadnavis, S., Karmacharya, J., Wienhold, F. G., Luo, B. P., Wernli, H., and Peter, T.: Water Vapor in the Asian Summer Monsoon Anticyclone: Comparison of Balloon-Borne Measurements and ECMWF Data, *J. Geophys. Res.-Atmos.*, 124, 7053–7068, <https://doi.org/10.1029/2018JD030000>, 2019.

- Brunamonti, S., Graf, M., Bühlmann, T., Pascale, C., Ilak, I., Emmenegger, L., and Tuzson, B.: SI-traceable validation of a laser spectrometer for balloon-borne measurements of water vapor in the upper atmosphere, *Atmos. Meas. Tech.*, 16, 4391–4407, <https://doi.org/10.5194/amt-16-4391-2023>, 2023.
- Brunamonti, S., Saathoff, H., Hertzog, A., Diskin, G., Fujiwara, M., Rosenlof, K., Möhler, O., Tuzson, B., Emmenegger, L., Amarouche, N., Durry, G., Frérot, F., Samake, J.-C., Cenac, C., Lopez, J., Monnier, P., and Ghysels, M.: Dataset for the AquaVIT-4 intercomparison of atmospheric hygrometers, Karlsruhe Institute of Technology [data set], <https://doi.org/10.35097/e7yxjpyc8xyv1ga4>, 2025.
- Buchholz, B. and Ebert, V.: Offsets in fiber-coupled diode laser hygrometers caused by parasitic absorption effects and their prevention, *Meas. Sci. Technol.*, 25, 75501, <https://doi.org/10.1088/0957-0233/25/7/075501>, 2014.
- Buchholz, B., Böse, N., and Ebert, V.: Absolute validation of a diode laser hygrometer via intercomparison with the German national primary water vapor standard, *Appl. Phys. B* 116, 883–899, <https://doi.org/10.1007/s00340-014-5775-4>, 2014.
- Carbone, S., D. Riviere, E., Ghysels, M., Burgalat, J., Durry, G., Amarouche, N., Podglajen, A., and Hertzog, A.: Influence of atmospheric waves and deep convection on water vapour in the equatorial lower stratosphere seen from long-duration balloon measurements, *Atmos. Chem. Phys.*, 25, 10603–10623, <https://doi.org/10.5194/acp-25-10603-2025>, 2025.
- Dessler, A. E., Zhang, Z., and Yang, P.: Water-vapor climate feedback inferred from climate fluctuations, 2003–2008, *Geophys. Res. Lett.*, 35, L20704, <https://doi.org/10.1029/2008GL035333>, 2008.
- Dessler, A. E., Schoeberl, M. R., Wang, T., Davis, S. M., and Rosenlof, K. H.: Stratospheric water vapor feedback, *P. Natl. Acad. Sci. USA*, 110, 18087–18091, <https://doi.org/10.1073/pnas.1310344110>, 2013.
- Dirksen, R.: R23 replacement (HP-2), GRUAN Implementation and Coordination Meeting (ICM-15), Bern, Switzerland, 11–15 March 2014, https://www.gruan.org/gruan/editor/documents/meetings/icm-15/pres/pres_0610b_Dirksen_R23.pdf (last access: 5 July 2025), 2024.
- Diskin, G. S., Podolske, J. R., Sachse, G. W., and Slate, T. A.: Open-path airborne tunable diode laser hygrometer, *Proc. SPIE* 4817, Diode Lasers and Applications in Atmospheric Sensing, <https://doi.org/10.1117/12.453736>, 2002.
- Donahue, N. M., Henry, K. M., Mentel, T. F., Kiendler-Scharr, A., Spindler, C., Bohn, B., Brauers, T., Dorn, H. P., Fuchs, H., Tillmann, R., Wahner, A., Saathoff, H., Naumann, K. H., Möhler, O., Leisner, T., Müller, L., Reinnig, M. C., Hoffmann, T., Salo, K., Hallquist, M., Frosch, M., Bilde, M., Tritscher, T., Barmet, P., Pra-plan, A. P., Carlo, P. F., Dommen, J., Prevot, A. S. H., and Baltensperger, U.: Aging of biogenic secondary organic aerosol via gas-phase OH radical reactions, *Proc. Natl. Acad. Sci. USA*, 109, 13503–13508, <https://doi.org/10.1073/pnas.1115186109>, 2012.
- Durry, G., Amarouche, N., Joly, L., Liu, X., Parvitte, B., and Zéninari, V.: Laser diode spectroscopy of H₂O at 2.63 μ m for atmospheric applications, *Appl. Phys. B-Lasers O.*, 90, 573–580, <https://doi.org/10.1007/s00340-007-2884-3>, 2008.
- Ebert, V., Teichert, H., Giesemann, C., Saathoff, H., and Schurath, U.: Fiber-coupled in situ laser absorption spectrometer for the selective detection of water vapor traces down to the ppb-level, *Tech. Mess.*, 72, 23–30, 2005.
- Fahey, D. W., Gao, R.-S., Möhler, O., Saathoff, H., Schiller, C., Ebert, V., Krämer, M., Peter, T., Amarouche, N., Avallone, L. M., Bauer, R., Bozóki, Z., Christensen, L. E., Davis, S. M., Durry, G., Dyroff, C., Herman, R. L., Hunsmann, S., Khaykin, S. M., Mackrodt, P., Meyer, J., Smith, J. B., Spelten, N., Troy, R. F., Vömel, H., Wagner, S., and Wienhold, F. G.: The AquaVIT-1 intercomparison of atmospheric water vapor measurement techniques, *Atmos. Meas. Tech.*, 7, 3177–3213, <https://doi.org/10.5194/amt-7-3177-2014>, 2014.
- Fischer, M., Tuzson, B., Hugi, A., Brönnimann, R., Kunz, A., Blaser, S., Rochat, M., Landry, O., Müller, A., and Emmenegger, L.: Intermittent operation of QC-lasers for mid-IR spectroscopy with low heat dissipation: tuning characteristics and driving electronics, *Opt. Express*, 22, 7014–7027, <https://doi.org/10.1364/OE.22.007014>, 2014.
- Forster, P., Storelvmo, T., Armour, K., Collins, W., Dufresne, J.-L., Frame, D., Lunt, D. J., Mauritsen, T., Palmer, M. D., Watanabe, M., Wild, M., and Zhang, H.: The Earth's Energy Budget, Climate Feedbacks, and Climate Sensitivity, in: *Climate Change 2021: The Physical Science Basis, Contribution of Working Group I to the Sixth Assessment Report of the Intergovernmental Panel on Climate Change*, edited by: Masson-Delmotte, V., Zhai, P., Pirani, A., Connors, S. L., Péan, C., Berger, S., Caud, N., Chen, Y., Goldfarb, L., Gomis, M. I., Huang, M., Leitzell, K., Lonnoy, E., Matthews, J. B. R., Maycock, T. K., Waterfield, T., Yelekçi, O., Yu, R., and Zhou, B., Cambridge University Press, Cambridge, UK and New York, NY, USA, 923–1054, <https://doi.org/10.1017/9781009157896.009>, 2021.
- Forster, P. M. de F. and Shine, K. P.: Stratospheric water vapour changes as a possible contributor to observed stratospheric cooling, *Geophys. Res. Lett.*, 26, 3309–3312, <https://doi.org/10.1029/1999GL010487>, 1999.
- Gao, L., Song, J., Mohr, C., Huang, W., Vallon, M., Jiang, F., Leisner, T., and Saathoff, H.: Kinetics, SOA yields, and chemical composition of secondary organic aerosol from β -caryophyllene ozonolysis with and without nitrogen oxides between 213 and 313 K, *Atmos. Chem. Phys.*, 22, 6001–6020, <https://doi.org/10.5194/acp-22-6001-2022>, 2022.
- GCOS: The 2022 GCOS Implementation Plan (GCOS-244), <https://library.wmo.int/idurl/4/58104> (last access: 23 January 2025), 2022.
- Ghysels, M., Riviere, E. D., Khaykin, S., Stoeffler, C., Amarouche, N., Pommereau, J.-P., Held, G., and Durry, G.: Intercomparison of in situ water vapor balloon-borne measurements from Pico-SDLA H₂O and FLASH-B in the tropical UTLS, *Atmos. Meas. Tech.*, 9, 1207–1219, <https://doi.org/10.5194/amt-9-1207-2016>, 2016.
- Ghysels, M., Durry, G., Amarouche, N., Hurst, D., Hall, E., Xiong, K., Dupont, J.-C., Samake, J.-C., Frérot, F., Bejjani, R., and Riviere, E. D.: Pico-Light H₂O: intercomparison of in situ water vapour measurements during the AsA 2022 campaign, *Atmos. Meas. Tech.*, 17, 3495–3513, <https://doi.org/10.5194/amt-17-3495-2024>, 2024.
- Gordon, I. E., Rothman, L. S., Hargreaves, R. J., Hashemi, R., Karlovets, E. V., Skinner, F. M., Conway, E. K., Hill, C., Kochanov, R. V., Tan, Y., Wcislo, P., Finenko, A. A., Nelson, K.,

- Bernath, P. F., Birk, M., Boudon, V., Campargue, A., Chance, K. V., Coustenis, A., Drouin, B. J., Flaud, J.-M., Gamache, R. R., Hodges, J. T., Jacquemart, D., Mlawer, E. J., Nikitin, A. V., Perevalov, V. I., Rotger, M., Tennyson, J., Toon, G. C., Tran, H., Tyuterev, V. G., Adkins, E. M., Baker, A., Barbe, A., Canè, E., Császár, A. G., Dudaryonok, A., Egorov, O., Fleisher, A. J., Fleurbaey, H., Foltynowicz, A., Furtenbacher, T., Harrison, J. J., Hartmann, J.-M., Horneman, V.-M., Huang, X., Karman, T., Karns, J., Kassi, S., Kleiner, I., Kofman, V., Kwabia-Tchana, F., Lavrentieva, N. N., Lee, T. J., Long, D. A., Lukashetskaya, A. A., Lyulin, O. M., Makhnev, V. Yu., Matt, W., Massie, S. T., Melosso, M., Mikhailenko, S. N., Mondelain, D., Müller, H. S. P., Naumenko, O. V., Perrin, A., Polyansky, O. L., Raddaoui, E., Raston, P. L., Reed, Z. D., Rey, M., Richard, C., Tóbiás, R., Sadiek, I., Schwenke, D. W., Starikova, E., Sung, K., Tamassia, F., Tashkun, S. A., Vander Auwera, J., Vasilenko, I. A., Vigasin, A. A., Villanueva, G. L., Vispoel, B., Wagner, G., Yachmenev, A., and Yurchenko, S. N.: The HITRAN2020 molecular spectroscopic database, *J. Quant. Spectrosc. Ra.*, 277, 107949, <https://doi.org/10.1016/j.jqsrt.2021.107949>, 2022.
- Graf, M., Emmenegger, L., and Tuzson, B.: Compact, circular, and optically stable multipass cell for mobile laser absorption spectroscopy, *Opt. Lett.*, 43, 2434–2437, <https://doi.org/10.1364/OL.43.002434>, 2018.
- Graf, M., Scheidegger, P., Kupferschmid, A., Looser, H., Peter, T., Dirksen, R., Emmenegger, L., and Tuzson, B.: Compact and lightweight mid-infrared laser spectrometer for balloon-borne water vapor measurements in the UTLS, *Atmos. Meas. Tech.*, 14, 1365–1378, <https://doi.org/10.5194/amt-14-1365-2021>, 2021.
- Hall, E. G., Jordan, A. F., Hurst, D. F., Oltmans, S. J., Vömel, H., Kühnreich, B., and Ebert, V.: Advancements, measurement uncertainties, and recent comparisons of the NOAA frost point hygrometer, *Atmos. Meas. Tech.*, 9, 4295–4310, <https://doi.org/10.5194/amt-9-4295-2016>, 2016.
- Hegglin, M. I., Tegtmeier, S., Anderson, J., Froidevaux, L., Fuller, R., Funke, B., Jones, A., Lingenfelter, G., Lumpe, J., Pendlebury, D., Remsberg, E., Rozanov, A., Toohey, M., Urban, J., von Clarmann, T., Walker, K. A., Wang, R., and Weigel, K.: SPARC Data Initiative: Comparison of water vapor climatologies from international satellite limb sounders, *J. Geophys. Res.-Atmos.*, 118, 11824–11846, <https://doi.org/10.1002/jgrd.50752>, 2013.
- Hurst, D., Lambert, A., Read, B., Davis, S., Rosenlof, K., Hall, E., Jordan, A., and Oltmans, S.: Validation of Aura Microwave Limb Sounder stratospheric water vapor measurements by the NOAA frost point hygrometer, *J. Geophys. Res.*, 119, 1612–1625, <https://doi.org/10.1002/2013JD020757>, 2014.
- Hurst, D. F., Oltmans, S. J., Vömel, H., Rosenlof, K. H., Davis, S. M., Ray, E. A., Hall, E. G., and Jordan, A. F.: Stratospheric water vapor trends over Boulder, Colorado: Analysis of the 30 year Boulder record, *J. Geophys. Res.-Atmos.*, 116, D02306, <https://doi.org/10.1029/2010JD015065>, 2011.
- Hurst, D. F., Read, W. G., Vömel, H., Selkirk, H. B., Rosenlof, K. H., Davis, S. M., Hall, E. G., Jordan, A. F., and Oltmans, S. J.: Recent divergences in stratospheric water vapor measurements by frost point hygrometers and the Aura Microwave Limb Sounder, *Atmos. Meas. Tech.*, 9, 4447–4457, <https://doi.org/10.5194/amt-9-4447-2016>, 2016.
- Hurst, D. F., Fujiwara, M., and Oltmans, S.: Chapter 3. Frost point hygrometers, in *Field Measurements for Passive Environmental Remote Sensing – Instrumentation, Intensive Campaigns, and Satellite Applications*, 1st Edition, edited by: Nalli, N., Elsevier, Radarweg, Netherlands, 436 pp., ISBN: 9780128239537, <https://doi.org/10.1016/B978-0-12-823953-7.00015-0>, 2022.
- Inai, Y., Shibata, T., Fujiwara, M., Hasebe, F., and Vömel, H.: High supersaturation inside cirrus in well-developed tropical tropopause layer over Indonesia, *Geophys. Res. Lett.*, 39, 20, <https://doi.org/10.1029/2012GL053638>, 2012.
- Kaufmann, S., Voigt, C., Heller, R., Jurkat-Witschas, T., Krämer, M., Rolf, C., Zöger, M., Giez, A., Buchholz, B., Ebert, V., Thornberry, T., and Schumann, U.: Intercomparison of midlatitude tropospheric and lower-stratospheric water vapor measurements and comparison to ECMWF humidity data, *Atmos. Chem. Phys.*, 18, 16729–16745, <https://doi.org/10.5194/acp-18-16729-2018>, 2018.
- Krämer, M., Schiller, C., Afchine, A., Bauer, R., Gensch, I., Mangold, A., Schlicht, S., Spelten, N., Sitnikov, N., Borrmann, S., de Reus, M., and Spichtinger, P.: Ice supersaturations and cirrus cloud crystal numbers, *Atmos. Chem. Phys.*, 9, 3505–3522, <https://doi.org/10.5194/acp-9-3505-2009>, 2009.
- Laborde, M., Schnaiter, M., Linke, C., Saathoff, H., Naumann, K.-H., Möhler, O., Berlenz, S., Wagner, U., Taylor, J. W., Liu, D., Flynn, M., Allan, J. D., Coe, H., Heimerl, K., Dahlkötter, F., Weinzierl, B., Wollny, A. G., Zannata, M., Cozic, J., Laj, P., Hitzenberger, R., Schwarz, J. P., and Gysel, M.: Single Particle Soot Photometer intercomparison at the AIDA chamber, *Atmos. Meas. Tech.*, 5, 3077–3097, <https://doi.org/10.5194/amt-5-3077-2012>, 2012.
- Lamb, K., Clouser, B., Bolot, B., Sarkozy, L., Ebert, V., Saathoff, H., Möhler, O., and Moyer, E.: Laboratory measurements of HDO/H₂O isotopic fractionation during ice deposition in simulated cirrus clouds, *Proc. Natl. Acad. Sci. USA*, 114, 5612–5617, <https://doi.org/10.1073/pnas.1618374114>, 2017.
- Lamb, K. D., Harrington, J. Y., Clouser, B. W., Moyer, E. J., Sarkozy, L., Ebert, V., Möhler, O., and Saathoff, H.: Re-evaluating cloud chamber constraints on depositional ice growth in cirrus clouds – Part 1: Model description and sensitivity tests, *Atmos. Chem. Phys.*, 23, 6043–6064, <https://doi.org/10.5194/acp-23-6043-2023>, 2023.
- Luo, B. P., Peter T., Fueglistaler, S., Wernli, H., Wirth, M., Kiemle, C., Flentje, H., Yushkov, V. A., Khattatov, V., Rudakov, V., Thomas, A., Borrmann, S., Toci, G., Mazzinghi, P., Beuermann, J., Schiller, C., Cairo, F., Di Donfrancesco, G., Adriani, A., Volk, C. M., Strom, J., Noone, K., Mitev, V., MacKenzie, R. A., Carslaw, K. S., Trautmann, T., Santacesaria, V., and Stefanutti, L.: Dehydration potential of ultrathin clouds at the tropical tropopause, *Geophys. Res. Lett.*, 30, 1557, <https://doi.org/10.1029/2002GL016737>, 2003.
- Maycock, A. C., Joshi, M. M., Shine, K. P., Davis, S. M., and Rosenlof, K. H.: The potential impact of changes in lower stratospheric water vapour on stratospheric temperatures over the past 30 years, *Q. J. R. Meteorol. Soc.*, 140, 2176–2185, <https://doi.org/10.1002/qj.2287>, 2014.
- Meyer, J., Rolf, C., Schiller, C., Rohs, S., Spelten, N., Afchine, A., Zöger, M., Sitnikov, N., Thornberry, T. D., Rollins, A. W., Bozóki, Z., Tátrai, D., Ebert, V., Kühnreich, B., Mackrodt, P., Möhler, O., Saathoff, H., Rosenlof, K. H., and Krämer, M.: Two decades of water vapor measurements with the FISH fluores-

- cence hygrometer: a review, *Atmos. Chem. Phys.*, 15, 8521–8538, <https://doi.org/10.5194/acp-15-8521-2015>, 2015.
- Möhler, O., Stetzer, O., Schaefers, S., Linke, C., Schnaiter, M., Tiede, R., Saathoff, H., Krämer, M., Mangold, A., Budz, P., Zink, P., Schreiner, J., Mauersberger, K., Haag, W., Kärcher, B., and Schurath, U.: Experimental investigation of homogeneous freezing of sulphuric acid particles in the aerosol chamber AIDA, *Atmos. Chem. Phys.*, 3, 211–223, <https://doi.org/10.5194/acp-3-211-2003>, 2003.
- Möhler, O., Benz, S., Saathoff, H., Schnaiter, M., Wagner, R., Schneider, J., Walter, S., Ebert, V., and Wagner, S.: The effect of organic coating on the heterogeneous ice nucleation activity of mineral dust aerosols, *Environ. Res. Lett.*, 3, 025007, <https://doi.org/10.1088/1748-9326/3/2/025007>, 2008.
- Murphy, D. M. and Koop, T.: Review of the vapour pressures of ice and supercooled water for atmospheric applications, *Q. J. R. Meteorol. Soc.*, 131, 1539–1565, <https://doi.org/10.1256/qj.04.94>, 2005.
- Nash, J., Oakley, T., Vömel, H., Wei, L., and World Meteorological Organization (WMO): IOM Report No. 107: WMO Intercomparison of High Quality Radiosonde Systems (12 July–3 August 2010), WMO, Geneva, 249 pp., WMO/TD-No. 1580, <https://library.wmo.int/idurl/4/50499> (last access: 24 February 2025), 2011.
- Oltmans, S., Rosenlof, K., Michelsen, H., Nedoluha, G., Pan, L., Read, W., Remsberg, E., and Schiller, C.: SPARC Report No. 2: Upper Tropospheric and Stratospheric Water Vapour, Chap. 2, Tech. rep., <https://www.sparc-climate.org/publications/sparc-reports/sparc-report-no-2/> (last access: 22 January 2025), 2000.
- Peter, T., Marcolli, C., Spichtinger, P., Corti, T., Baker, M. B., and Koop, T.: When Dry Air Is Too Humid, *Science*, 314, 1399–1402, <https://doi.org/10.1126/science.1135199>, 2006.
- Poltera, Y., Luo, B., Wienhold, F. G., and Peter, T.: Observations of water vapor in the UT/LS of unprecedented accuracy with non-equilibrium corrected frost point hygrometers, EGU General Assembly 2025, Vienna, Austria, 27 Apr–2 May 2025, EGU25-19811, <https://doi.org/10.5194/egusphere-egu25-19811>, 2025.
- Randel, W. and Park, M.: Diagnosing Observed Stratospheric Water Vapor Relationships to the Cold Point Tropopause, *J. Geophys. Res. Atmos.*, 124, 7018–7033, <https://doi.org/10.1029/2019JD030648>, 2019.
- Riese, M., Ploeger, F., Rap, A., Vogel, B., Konopka, P., Dameris, M., and Forster, P.: Impacts of uncertainties in atmospheric mixing on simulated UTLS composition and related radiative effects, *J. Geophys. Res.-Atmos.*, 117, D16305, <https://doi.org/10.1029/2012JD017751>, 2012.
- Rolf, C., Khordakova, D., and Vömel, H.: CFH cooling agent alternatives, GRUAN Implementation and Coordination Meeting (ICM-12), 16–20 November 2020, https://www.gruan.org/gruan/editor/documents/meetings/icm-12/pres/pres_302_Rolf_CFH_Cooling-Agent-Tests.pdf (last access: 5 July 2025), 2020.
- Rollins, A. W., Thornberry, T., Gao, R. S., Smith, J. B., Sayres, D. S., Sargent, M. R., Schiller, C., Krämer, M., Spelten, N., Hurst, D. F., Jordan, A. F., Hall, E. G., Vömel, H., Diskin, G. S., Podolske, J. R., Christensen, L. E., Rosenlof, K. H., Jensen, E. J., and Fahey, D. W.: Evaluation of UT/LS hygrometer accuracy by intercomparison during the NASA MACPEX mission, *J. Geophys. Res.-Atmos.*, 119, 1915–1935, <https://doi.org/10.1002/2013JD020817>, 2014.
- Rosenlof, K. H., Oltmans, S. J., Kley, D., Russell III, J. M., Chiou, E.-W., Chu, W. P., Johnson, D. G., Kelly, K. K., Michelsen, H. A., Nedoluha, G. E., Remsberg, E. E., Toon, G. C., and McCormick, M. P.: Stratospheric water vapor increases over the past half-century, *Geophys. Res. Lett.*, 28, 1195–1198, <https://doi.org/10.1029/2000GL012502>, 2001.
- Rothman, L. S., Gordon, I. E., Babikov, Y., Barbe, A., Chris Benner, D., Bernath, P. F., Birk, M., Bizzocchi, L., Boudon, V., Brown, L. R., Campargue, A., Chance, K., Cohen, E. A., Coudert, L. H., Devi, V. M., Drouin, B. J., Fayt, A., Flaud, J.-M., Gamache, R. R., Harrison, J. J., Hartmann, J.-M., Hill, C., Hodges, J. T., Jacquemart, D., Jolly, J. Lamouroux, J., Le Roy, R. J., Li, G., Long, D. A., Lyulin, O. M., Mackie, C. J., Massie, S. T., Mikhailenko, S., Müller, H. S. P., Naumenko, O. V., Nikitin, A. V., Orphal, J., Perevalov, V., Perrin, A., Polovtseva, E. R., Richard, C., Smith, M. A. H., Starikova, E., Sung, K., Tashkun, S., Tennyson, J., Toon, G. C., Tyuterev, V. G., and Wagner, G.: The HITRAN2012 molecular spectroscopic database, *J. Quant. Spectrosc. Radiat. Transf.*, 130, 4–50, <https://doi.org/10.1016/j.jqsrt.2013.07.002>, 2013.
- Sarkozy, L. C., Clouser, B. W., Lamb, K. D., Stutz, E. J., Saathoff, A. H., Möhler, O., Ebert, V., and Moyer, E. J.: The Chicago Water Isotope Spectrometer (ChiWIS-lab): A tunable diode laser spectrometer for chamber-based measurements of water vapor isotopic evolution during cirrus formation, *Rev. Sci. Instrum.* 91, 045120, <https://doi.org/10.1063/1.5139244>, 2020.
- Scherer, M., Vömel, H., Fueglistaler, S., Oltmans, S. J., and Staehelin, J.: Trends and variability of midlatitude stratospheric water vapour deduced from the re-evaluated Boulder balloon series and HALOE, *Atmos. Chem. Phys.*, 8, 1391–1402, <https://doi.org/10.5194/acp-8-1391-2008>, 2008.
- Shen, X., Bell, D. M., Coe, H., Hiranuma, N., Mahrt, F., Marsden, N. A., Mohr, C., Murphy, D. M., Saathoff, H., Schneider, J., Wilson, J., Zawadowicz, M. A., Zelenyuk, A., DeMott, P. J., Möhler, O., and Cziczo, D. J.: Measurement report: The Fifth International Workshop on Ice Nucleation phase 1 (FIN-01): intercomparison of single-particle mass spectrometers, *Atmos. Chem. Phys.*, 24, 10869–10891, <https://doi.org/10.5194/acp-24-10869-2024>, 2024.
- Singer, C. E., Clouser, B. W., Khaykin, S. M., Krämer, M., Cairo, F., Peter, T., Lykov, A., Rolf, C., Spelten, N., Afchine, A., Brunamonti, S., and Moyer, E. J.: Intercomparison of upper tropospheric and lower stratospheric water vapor measurements over the Asian Summer Monsoon during the StratoClim campaign, *Atmos. Meas. Tech.*, 15, 4767–4783, <https://doi.org/10.5194/amt-15-4767-2022>, 2022.
- Sitnikov, N. M., Yushkov, V. A., Afchine, A., Korshunov, L. I., Astakhov, V. I., Ulanovskii, A. E., Kraemer, M., Mangold, A., Schiller, C., and Ravegnani, F.: The FLASH instrument for water vapor measurements on board the high-altitude airplane, *Instruments and Experimental Techniques*, 50, 113–121, <https://doi.org/10.1134/S0020441207010174>, 2007.
- Skrotzki, J.: High-accuracy multiphase humidity measurements using TDLAS: application to the investigation of ice growth in simulated cirrus clouds, Diss. Submitted to the University of Heidelberg, <https://archiv.ub.uni-heidelberg.de/volltextserver/13141/> (last access: 7 October 2025), 2012.

- Skrotzki, J., Connolly, P., Schnaiter, M., Saathoff, H., Möhler, O., Wagner, R., Niemand, M., Ebert, V., and Leisner, T.: The accommodation coefficient of water molecules on ice – cirrus cloud studies at the AIDA simulation chamber, *Atmos. Chem. Phys.*, 13, 4451–4466, <https://doi.org/10.5194/acp-13-4451-2013>, 2013.
- Soden, B. J., Jackson, D. L., Ramaswamy, V., Schwarzkopf, M. D., and Huang, X.: The Radiative Signature of Upper Tropospheric Moistening, *Science*, 310, 841–844, <https://doi.org/10.1126/science.1115602>, 2005.
- Solomon, S., Rosenlof, K. H., Portmann, R. W., Daniel, J. S., Davis, S. M., Sanford, T. J., and Plattner, G.-K.: Contributions of stratospheric water vapor to decadal changes in the rate of global warming, *Science*, 327, 1219–1223, <https://doi.org/10.1126/science.1182488>, 2010.
- Stenke, A. and Grewe, V.: Simulation of stratospheric water vapor trends: impact on stratospheric ozone chemistry, *Atmos. Chem. Phys.*, 5, 1257–1272, <https://doi.org/10.5194/acp-5-1257-2005>, 2005.
- Tao, M., Konopka, P., Wright, J. S., Liu, Y., Bian, J., Davis, S. M., Jia, Y., and Ploeger, F.: Multi-decadal variability controls short-term stratospheric water vapor trends, *Commun. Earth Environ.*, 4, 441, <https://doi.org/10.1038/s43247-023-01094-9>, 2023.
- Tian, E. W., Su, H., Tian, B., and Jiang, J. H.: Interannual variations of water vapor in the tropical upper troposphere and the lower and middle stratosphere and their connections to ENSO and QBO, *Atmos. Chem. Phys.*, 19, 9913–9926, <https://doi.org/10.5194/acp-19-9913-2019>, 2019.
- UNEP: Montreal Protocol – Kigali Amendment, chap. XXVII, 2. f. Amendment to the Montreal Protocol on Substances that Deplete the Ozone Layer, Kigali, Rwanda, https://treaties.un.org/doc/Treaties/2016/10/2016101503-23PM/Ch_XXVII-2.f-EnglishandFrench.pdf (last access: 22 January 2025), 2016.
- Vömel, H., David, D. E., and Smith, K.: Accuracy of tropospheric and stratospheric water vapor measurements by the cryogenic frost point hygrometer: Instrumental details and observations, *J. Geophys. Res.-Atmos.*, 112, D08305, <https://doi.org/10.1029/2006JD007224>, 2007.
- Vömel, H., Naebert, T., Dirksen, R., and Sommer, M.: An update on the uncertainties of water vapor measurements using cryogenic frost point hygrometers, *Atmos. Meas. Tech.*, 9, 3755–3768, <https://doi.org/10.5194/amt-9-3755-2016>, 2016.
- Wagner, R., Benz, S., Möhler, O., Saathoff, H., and Schurath, U.: Probing ice clouds by broadband mid-infrared extinction spectroscopy: case studies from ice nucleation experiments in the AIDA aerosol and cloud chamber, *Atmos. Chem. Phys.*, 6, 4775–4800, <https://doi.org/10.5194/acp-6-4775-2006>, 2006.
- Wagner, R., Linke, C., Naumann, K.-H., Schnaiter, M., Vragel, M., Gangl, M., and Horvath, H.: A review of optical measurements at the aerosol and cloud chamber AIDA, *J. Quant. Spectrosc. Radiat. Transf.*, 110, 930–949, <https://doi.org/10.1016/j.jqsrt.2009.01.026>, 2009.
- Zöger, M., Afchine, A., Eicke, N., Gerhards, M.-T., Klein, E., McKenna, D. S., Mörschel, U., Schmidt, U., Tan, V., Tuitjer, F., Woyke, T., and Schiller, C.: Fast in situ stratospheric hygrometers: A new family of balloon-borne Lyman α photofragment fluorescence hygrometers, *J. Geophys. Res.*, 104, 1807–1816, 1999.